

Unveiling the Face-Dependent Ice Growth Kinetics: Insights from Molecular Dynamics on the Basal and Prism Surfaces

Jihong Shi,¹ Maxwell Fulford,¹ Matteo Salvalaglio,² and Carla Molteni^{*1}

¹⁾*Department of Physics, King's College London, Strand, London WC2R 2LS, UK.*

²⁾*Department of Chemical Engineering, University College London, Torrington Place, London WC1E 7JE, UK.*

(*Electronic mail: carla.molteni@kcl.ac.uk)

(Dated: 14 October 2024)

Ice nucleation and growth are critical in many fields, including atmospheric science, cryobiology, and aviation. However, understanding the detailed mechanisms of ice crystal growth remains challenging. In this work, crystallization at the ice/quasi-liquid layer (QLL) interface of the basal and primary prism (prism1) surfaces of hexagonal ice (Ih) was investigated using molecular dynamics simulations across a wide range of temperatures for the TIP4P/Ice model, with comparisons to the mW coarse-grained model. Together with elucidating the temperature-dependent mechanisms of crystallization, face-specific growth rates were systematically estimated. While the prism surface generally exhibits faster growth rates than the basal surface, a temperature-dependent crossover in growth rates between the basal and prism surfaces is observed in TIP4P/Ice simulations, which correlates with a crossover in QLL thickness and with the well-known column to platelets transition in ice-crystal habits at low vapour pressure. This observation helps decode the complex dependence between crystal morphology and temperature in ice crystals.

I. INTRODUCTION

Understanding ice nucleation and regulating ice growth is important for a range of fields, including cryobiology^{1,2}, cryopreservation^{3,4}, the aviation industry^{5,6}, and atmospheric science^{7,8}. Even though the characteristics of ice and water have been known for decades, insights into ice crystal growth remain elusive.

Ice crystal growth is a competitive process between molecular ordering and disordering aided by diffusion^{9,10}. The driving forces of supercooling for crystallization become more significant as the temperature gradually decreases from the melting point of ice. On the contrary, lowering the temperature reduces the diffusion capacity of molecules, and weaker liquid mobility would be detrimental to ice growth. Thus, mutually opposite effects act on ice growth as the temperature changes. In this work, we aim to unravel the ice crystal growth mechanism and kinetics on different hexagonal ice (Ih) surfaces as a function of temperature using molecular dynamics (MD) simulations.

Ice crystals predominantly grow in two types of environmental conditions: supercooled water and supersaturated water vapour¹¹. However, the presence of a quasi-liquid layer¹² (QLL), which develops at ice surfaces in the vapour environment, blurs this distinction, as an interface with the liquid exists at both the ice-QLL-vapour and liquid-ice interfaces. At the liquid-ice interface, water molecules from the liquid phase organize into the crystalline structure of ice, growing the ice crystal. This is a direct phase transition from liquid to solid in the melt phase. Similarly, the presence of the QLL between the vapour and ice phases facilitates ice growth from the vapour phase because it allows for the diffusion and condensation of water vapour molecules onto the ice surface¹³, which then integrates into the ice lattice. Our simulation model in this study starts from the equilibrium state of QLL on the ice Ih surfaces, which is then extended to observe the ice crys-

tal growth process and mechanism at these complex interfaces. While the basal Ih face grows from both liquid and vapour, in the first environment, the relevant prismatic face is the secondary one (prism2), while in the second, it is the primary one (prism1)¹⁴. Hence, we concentrated on the basal and prism1 surfaces, as we are interested in the intriguing temperature-dependent hexagonal prism morphologies of ice crystal at low vapour pressure, growing as plate-like, column-like, plate-like, and then column-like again as temperature decreases^{11,13,15,16}.

Extensive experimental observations of ice growth were carried out using different optical microscopy techniques^{17–19}. Bright-field microscopy and Mach-Zehnder interferometry^{20,21} were subsequently used to determine the growth rates for the ice Ih basal and prism1 surfaces. These approaches enable precise measurements of the growth rate at the nanometre/s scale and the three-dimensional surface structure of ice crystals. Recently, Sazaki *et al.*²² used advanced optical microscopy techniques, laser confocal microscopy combined with differential interference contrast microscopy (LCM-DIM), and visualized a 2D nucleation and screw dislocations growth mechanisms on the ice Ih basal surface; the temperature dependence of growth kinetics and the role of surface diffusion of water molecules were discussed. They demonstrated the significant role of surface diffusion of water molecules on a basal face in the lateral growth of elementary steps when the distance between adjacent spiral steps is smaller than 15 μm . Miyamoto *et al.*²³ observed the growth of elementary spiral steps on the ice Ih prism faces heteroepitaxially grown on a CdSe substrate using LCM-DIM. The most significant finding was that screw dislocations on prism faces are primarily located in the interiors of the faces, in contrast with basal faces where dislocations are found at the edges. This advanced experimental technique highlighted significant differences in growth behaviours between the prism and basal faces of ice Ih crystals. Advances and developments in optical

science and technology have all contributed to furthering our understanding of ice growth kinetics.

Numerous computer simulations were performed to determine the ice crystal growth rate on different surfaces/interfaces. In early MD simulations, Carignano et al.²⁴ led the first comparison MD study of hexagonal ice growth from pure water and a brine solution. By building the bulk systems with the interface at the basal and the prism1 plane of ice, they found that the ice growth is faster on the prismatic plane than on the basal plane. Still, in these cases, only the growth of ice at the ice-liquid interface in bulk with periodic boundary conditions imposed in all three directions of the systems was considered, and the subcooling was only considered up to -18 K. In the same year, Nada et al.²⁵ carried out MD simulations to study the growth of different surfaces of ice Ih from supercooled water in a bulk system containing two ice-liquid interfaces. They also found that the growth rate on the second prismatic plane was more significant than that on the primary prismatic and basal surfaces; however, the calculation only explored a single temperature at 268 K. Later, Razul et al.²⁶ carried out ice growth studies on different interfaces of ice Ih and cubic ice (ice Ic) in bulk systems using the TIP4P, TIP4P-Ew, and SPC/E water models, with the various water models revealing higher growth rates for both prismatic surfaces than for the basal surface in the -65 to -40 K supercooling interval. A study of ice growth at 260 K using the TIP5P-E water model for different-sized ice Ih surfaces similarly confirmed that the basal surface at different system scales has the lowest growth rate compared to the other investigated prismatic surfaces; differences were analyzed in terms of transient structures during the crystallization process²⁷. Rozmanov et al.¹⁰ also examined the ice growth on ice-liquid interfaces in the bulk systems using the TIP4P-2005 water model at temperatures ranging from -40 to +16 K with respect to the melting temperature. At around 12 K below the melting temperature, the growth rates approach a maximum value of 0.7 to 1.1 Å/ns for the system with "large" ($2.7 \times 3.1 \text{ nm}^2$) and "small" ($1.8 \times 1.6 \text{ nm}^2$) interface size²⁸.

The modelling at the atomistic level of ice growth kinetics and understanding of the underlying mechanisms have been developing for several years and are still evolving. Nada and Furukawa presented the first simulation study involving the discussion of ice Ih growth kinetics and mechanisms²⁹. This study proposed that ice grows following a '*layer-by-layer*' mechanism on the basal surface, but according to a '*collected molecule*' process on the primary prism surface. However, the simulation time used in this study was relatively short due to computational limitations. The following year, the same group analyzed the translational and orientational order of the oxygen atoms to provide a more detailed explanation of the two types of growth mechanisms on the two surfaces of hexagonal ice³⁰. These findings have provided a solid foundation for subsequent research on ice growth kinetics. Matsumoto et al.³¹ made an interesting discovery through simulations, finding that the key to ice growth relies on long-lived and sufficiently numerous hydrogen-bonded stable structures in the evolution of the structures. Later, Carignano et al.²⁴ and Nada et al.²⁵ discovered another interesting interface phe-

nomenon through longer simulations. The solid substrate (ice) grown on the prismatic surface exhibits a geometrically rough state at the ice-water interface. In contrast, the solid substrate exhibits a molecularly flat state on the basal surface. Moore and Molinero³² did extensive work developing the mW model³³ and assessed the reliability of applying this model to ice growth kinetics studies. They argued that critical ice nuclei with less than ten water molecules develop faster than necessary for the liquid to relax, implying that supercooled liquid water cannot be adequately equilibrated. This has guided subsequent ice growth studies using this coarse-grained water model.

In summary, there is still no consensus on growth rates at different ice Ih surfaces both in experimental and theoretical/computational research, with a significant portion of studies focusing on narrow temperature ranges. Hence, further studies are needed to systematically determine how the ice growth rate trends with temperature over a wide range of supercooling temperatures. In fact, almost all the molecular simulation studies described above probe the ice crystal growth problem using models that incorporate ice-water interfaces in the bulk system, thus not addressing the effect of the QLL on the ice crystal growth. As discussed previously, the existence of the QLL changes the ice-water interface to the more complex ice-QLL-vapour double interface, and this structure allows the ice growth process to be not just the crystallization of supercooled water but rather the deposition of vapour on top of the QLL leading to QLL instability and crystallization at the QLL-ice interface.

The novelty of our work consists of investigating the kinetics of growth at surfaces including the QLL³⁴ rather than at bulk liquid-ice interfaces in a wide temperature range. Moreover, we clarified the evolution of the ice crystal morphologies between plate-like and column-like, which is linked to the temperature dependence of the growth rate. Atomistic configurations were generated through MD simulations with the TIP4P/Ice and mW model for the basal and prism1 crystal faces of ice Ih, in the temperature range between 240 K and 270 K for the TIP4P/Ice model³⁵ and between 200 K and 270 K for the mW model³³ used for comparison. We used a local Steinhardt order parameter (SOP) lq_3 , which we previously assessed for efficiency and accuracy, to distinguish between ice-like and liquid-like molecules³⁴.

II. METHODOLOGY

A. Ice Slab Modelling

Molecular dynamics simulations were performed using the rigid four-site TIP4P/Ice water model that was designed to study crystalline and amorphous ice phases to accurately reproduce the water phase diagram and the densities of several ice structures^{35,36}. Calculations with this model yield a melting temperature of ice Ih of 272.2 K at 1 bar, which closely approximates experimental value³⁶. Hydrogens were initially in a disordered configuration determined by a Monte Carlo procedure to minimize the supercell dipole moment while obey-

ing the Bernal-Fowler rule for hydrogen bonding^{37,38}. The coarse-grained mW model³³, which allows faster simulations, was also used for comparison.

Two ice Ih slabs composed of 5,760 water molecules were considered: one exposed the basal face (0001) to vacuum, while the other exposed the prism1 face (1010). As periodic boundary conditions were applied in all three directions, a vacuum layer was added by elongating the dimension of the box by 40 Å in the direction perpendicular to the exposed surface, producing two equivalent ice/vacuum interfaces. The size of the vacuum layer was chosen to be large enough so that the two ice/vacuum interfaces do not interact. Similarly, the length of the slab was chosen so that the two QLLs do not influence each other, especially at the higher temperatures, resulting, before equilibration, in a slab of the total size of $45.18 \times 46.98 \times 130.00 \text{ \AA}^3$ for basal surface and of $45.17 \times 133.00 \times 44.36 \text{ \AA}^3$ for prism surface at 260 K, respectively, as shown in Fig. 1. The basal slab consisted of 48 layers, each composed of 120 molecules, arranged in pairs with the intra-bilayer spacing of 0.93 Å and inter-bilayer spacing of 3.74 Å; the primary prism slab consisted of 48 layers of 120 atoms each, also arranged in pairs, with the intra-bilayer spacing of 1.30 Å and inter-bilayer spacing of 2.77 Å.

B. Molecular Dynamics Simulations

We started from the ice slabs in the QLL equilibrium state obtained by MD simulations as described in Ref³⁴. MD simulations were carried out up to 160 ns using the large-scale atomic/molecular massively parallel simulator (LAMMPS, Mar 03, 2020 version) package³⁹ in the NVT ensemble. For the TIP4P model, the cutoff for the long-range Coulomb and Van der Waals interactions was set as 12 Å, and a time step of 1 fs was used. For the mW model, a timestep of 1 fs was used. The temperature was controlled by a Nosé-Hoover thermostat with a relaxation time of 100 fs at 240 K, 245 K, 250 K, 255 K, 260 K, 265 K, and 270 K for TIP4P/Ice and at 200 K, 210 K, 220 K, 230 K, 240 K, 245 K, 250 K, 255 K, 260 K, 265 K, and 270 K for mW.

To imitate the conditions triggered by increasing the QLL thickness due to the absorption of water molecules, we artificially melted additional layers so that the QLL size was substantially larger than at equilibrium and then recrystallized during MD simulations. For the TIP4P model, the enlarged QLL was achieved by rapidly melting another eight ice layers for 2 ns at 300 K at one end of the ice slab while keeping the remaining atoms fixed at their original places (in practice, melting atoms with coordinates perpendicular to the surface between 60 and 105 Å), a region also containing some part of vacuum). After melting, the QLL/ice region's temperature was returned to our target supercooled temperature. The atoms in the ice region were kept rigid, and this process was run for 1 ns. The QLL/ice interface was thus relaxed with all constraints removed by first performing a short MD with timestep ranging from 0.01 to 1 fs (100,000 steps with 0.01 fs, 100,000 with 0.1 fs and 10,000 with 1 fs). Ice molecules at the QLL/ice interface could change their locations throughout

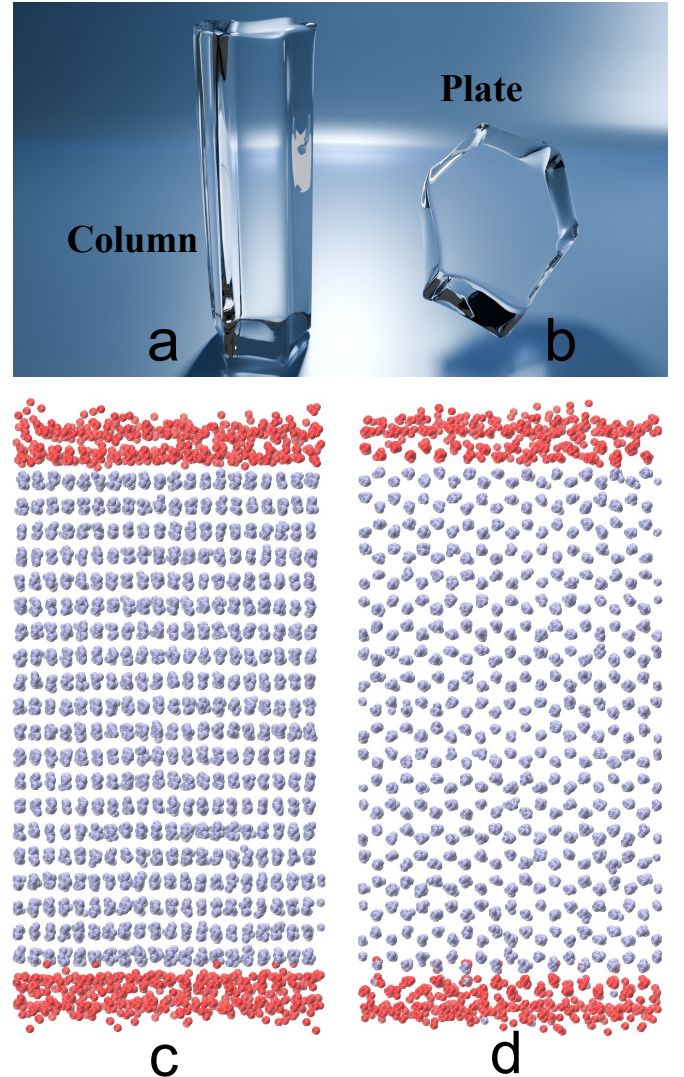


FIG. 1. Column-like (a) and plate-like (b) morphologies for ice Ih crystals. If the growth along the basal surface direction is faster than along the prism1 surface direction, the crystal morphology would be column-like, while it would be plate-like if the reverse is true. The slab models used to study the basal (c) and primary prismatic (d) surfaces of ice Ih in an exemplary MD snapshot with TIP4P/Ice at 260 K. Only oxygen atoms are shown, with those liquid-like in red to highlight the QLL and the remaining in blue.

these steps, but the system did not recrystallize due to the tiny time step. The initial time step was chosen small at 0.01 fs to ensure the system reaches a stable state without introducing large fluctuations. Fine-tuning the time step helps gently bring the system to equilibrium, after which the time step can be safely increased to 1 fs again. NVT simulations were then carried out for up to 160 ns until the QLL returned to equilibrium upon recrystallization. To improve statistics, three repeat simulations were performed at each temperature. The MD replicas use different random number seeds to initialize the velocities in the QLL melting and QLL/ice interface relax-

ation stages.

The simulation protocol for the QLL crystallization simulations with the mW model was similar to that with TIP4P/Ice. However, we observed that the system recrystallized during equilibrium at the target temperature, so it is difficult for this coarse-grained water model to complete the relaxation protocol without starting the crystallization process³³. Simulations of the QLL recrystallization were carried out for up to 3 ns for mW, given that the QLL crystallization happened substantially faster than with TIP4P/Ice; at variance from the mW MD, crystallization simulations used the smaller timestep of 1 fs. 10 replicas were simulated at each temperature.

We used the local Steinhardt order parameter lq_3 as implemented in PLUMED 2.7.3^{40,41} to distinguish between ice-like and liquid-like molecules with a cutoff for the first nearest neighbours of 3.5 Å and a threshold value of -0.67, as it shows a favourable ratio between accuracy and computational efficiency with respect to other classification methods, as previously discussed in Ref³⁴.

The open-source software Blender (version 4.1.1)⁴² was used to draw exemplary ice crystal plate-like and column-like morphologies.

III. RESULTS AND DISCUSSION

A. Temperature dependence of the growth rate at the QLL/ice interface

To estimate the ice growth rate for the different ice Ih surfaces, we monitored the evolution of the number of liquid-like molecules n_l and related it to the speed at which n_l decreases in time. Fig. S2(c) shows the time evolution of the excess number of liquid-like molecules (Δn_l) on the ice Ih basal surface using the TIP4P/Ice model. Δn_l is obtained from the simulations using $\Delta n_l(t) = n_l(t) - \text{min}(n_l)$. The inner images from (a) to (b) illustrate the recrystallization process at 260 K for the basal surface; similar data for the prism1 surface are shown in the supplementary information (SI) Fig. S1. The initial liquid-like region (in red) on the top surface that has been artificially melted is considerably larger than the equilibrium of the QLL on the bottom surface (Fig. 2a). The final configuration of the top surface at the end of the simulation is now similar to the bottom surface, confirming that crystallization has occurred. The melted QLL has returned to equilibrium (Fig. 2b). The decrease in n_l is continuous, and its trend is approximately linear.

The time-evolution of Δn_l is also shown in the SI Fig. S2 for both basal and prism1 surfaces and both TIP4P/Ice (Fig. S2a and S2b) and mW (Fig. S2c and S2d) at each simulated temperature for one of the replicas. The mW crystallization process is remarkably rapid at a time scale between 1 and 2 ns, with respect to 160 ns for TIP4P/Ice. Crystallization occurs even during the relaxation period, consistently with findings by Molinero et al.³², arguing that supercooled water using the mW model cannot be properly equilibrated due to the rapid crystallization process during the relaxation stage. In both water models, the time-evolution curves fluctuate con-

siderably at the highest temperature of 270 K, which is very close to the melting point.

The TIP4P/Ice and mW growth rates are estimated using a piecewise linear fitting technique from the Δn_l slope. The piecewise fitting procedure consists of three steps: The first step uses the Savitzky-Golay filter⁴⁵ (using polynomial fitting within each 200 data window) to smooth the raw data; the second step uses a dynamic programming method⁴⁶ to find the breakpoint where the slope of the curve changes significantly; the third step divides the fitting interval according to the breakpoint. The first decreasing trend fitting curves (the fitting curve before the breakpoint) appear to obtain the ice growth rate. The slope from the fitting is then converted into a volumetric growth rate and eventually into a thickness growth rate. The thickness d in Å was obtained as

$$d = \frac{\Delta \bar{n}_l M}{2\rho N_{AV} S 10^{-24}},$$

previously used to evaluate the QLL thickness from the number of liquid-like molecules in³⁴; here $M = 18.01574 \text{ g mol}^{-1}$ is the molecular weight of water, N_{AV} is the Avogadro number, ρ is the density of water in units of g cm^{-3} , and S is the size of the ice surface exposed to vacuum.

This fitting procedure significantly reduces the errors caused by an arbitrary artificial selection of the start and end points for the fitting; it is an upgrade on the linear fitting employed, for example, in Ref.⁴⁷ and⁴⁸. Only data for the growth process on the basal surface at 260 K are shown in Fig. S2c as an example; further data and fitting at different temperatures and surfaces are shown in the SI Fig. S3-S9. The temperatures at the extremes (240 K and 270 K) are those that behave less regularly due to the unbalance between the competing effects in the growth process.

The TIP4P/Ice ice growth rates of the basal and prism1 surfaces as a function of temperature are shown in Fig. S2d. The growth rates for the control mW model of these two surfaces are shown in Fig. 3. The rates were averaged over three replicas for TIP4P/Ice and ten replicas for mW. The error bars indicated the standard deviations of the replicas. The crystallization rate shows a gradual increase and then a gradual decrease with temperature. It reaches a maximum of 260 K (TIP4P/Ice) and 240 K (mW) for both basal and prism surfaces. This is due to the interplay between the interface chemical potential and diffusion, which have opposite trends with temperature²⁸ as explained in more detail below. We observe differences between the temperature dependence of the growth rate of mW with respect to that of the TIP4P/Ice model.

For the TIP4P/Ice simulations, low growth rates on different ice surfaces are found at both low temperatures of 240 K and high temperatures of 270 K (Fig. 2d). At the highest temperature of 270 K, as shown in the SI Fig. S9, the liquid-like molecules in the QLL show a slight growth trend at the beginning and then start to crystallize with a decreasing trend, with fluctuations consistent with the proximity to the melting temperature. A high level of supercooling leads to an easier transition from water to ice. However, at low temperatures, the thermal movement of molecules is decreased, so the clustering, collision, and ordering of molecules needed for

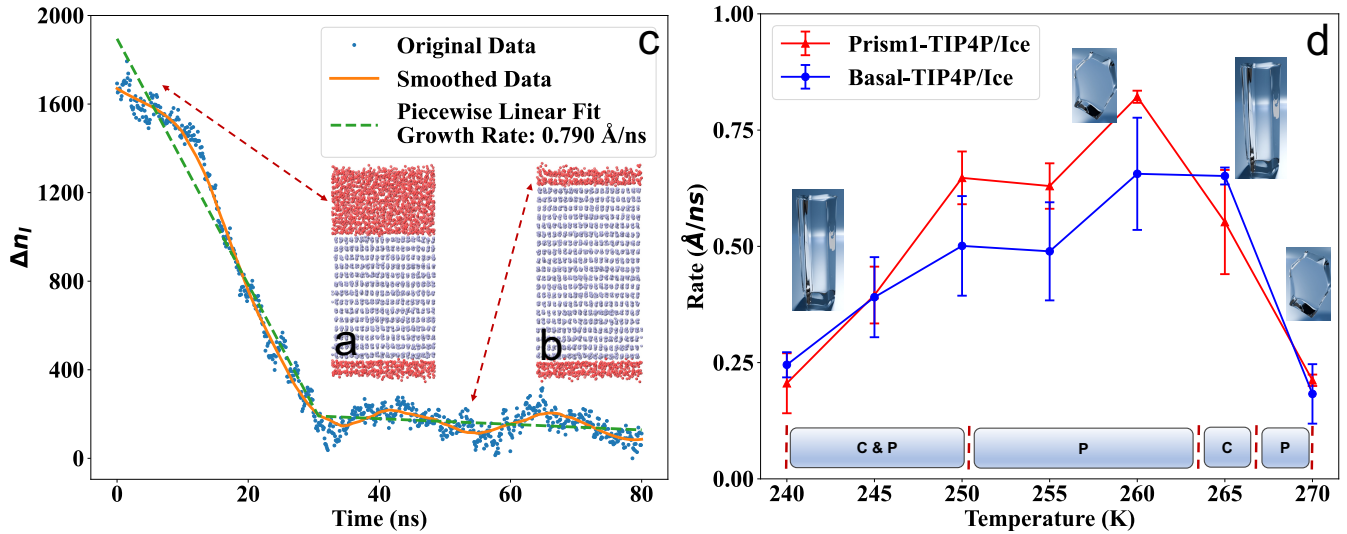


FIG. 2. The initial (a) and the final (b) structures in an 80 ns recrystallization simulation at 260 K for the basal face. The liquid-like molecules are coloured in red, and the ice-like molecules are in blue. Only oxygen atoms are shown. Time-evolution of the number of excess liquid-like molecules Δn_l during the TIP4P/Ice crystallization simulations of the ice Ih basal (c) surface at 260 K and illustration of the piecewise linear fitting technique used to obtain the ice growth rates. Growth rates for the basal (blue) and prism1 (red) surface with TIP4P/Ice (d) averaged over replicas. Suggested morphologies compatible with our rates are shown in (d); the morphology images taken from Fig. 1a and 1b do not intend to represent correct dimensions. The morphologies change for the TIP4P/Ice corresponds to the Nakaya Diagram⁴³. The vertical dashed lines in (d) delineating temperature intervals are based on the Nakaya Diagram⁴³ (labels C and P are column-like and plate-like, respectively), originally built by Ukihiro Nakaya and coworkers through experimental observations in the 1930s^{15,44}.

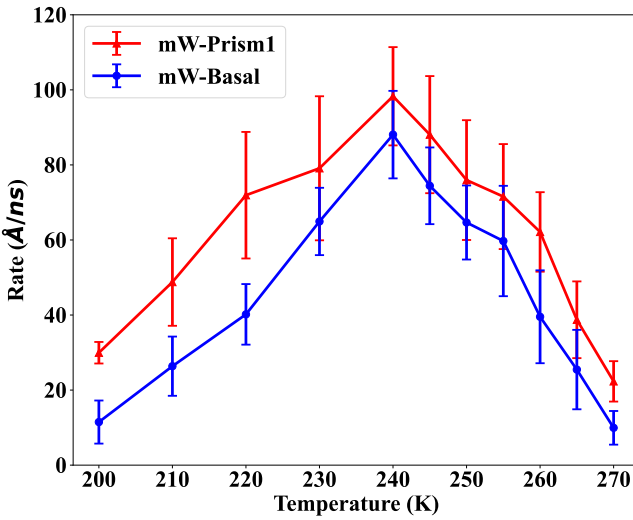


FIG. 3. Growth rates with temperature from 200 K to 270 K for the basal (blue) and prism1 (red) surfaces of the mW model averaged over replicas.

ice growth are weakened, leading to a reduction in the growth rate. On the other side of the range, at a low supercooling of 270 K, the substantial thermal movement of the molecules causes the newly formed regularly arranged ice structure to disintegrate. This slows down the ice growth rate. A similar scenario also applies to the case of the mW model at low and high supercooling, as shown in Fig. 3, although mW peaks at

240 K, which is different from TIP4P/Ice. In the mW model, the absence of explicit hydrogen atoms leads to lower diffusion energy barriers and much faster dynamics⁴⁹, resulting in significantly larger rates of QLL crystallization compared to TIP4P/Ice. Overall, the growth rate of the prism1 surface is greater than that of the basal surface over a wide range of temperatures (always in the case of mW). To clarify the reasons for the faster crystallization rate of the prism compared to the basal at some temperatures^{25,26}, we will explore the ice growth kinetics on different ice surfaces below.

The growth rates from our TIP4P/Ice simulations range from 0.2 to 1.0 Å/ns for both the basal and prism1 surfaces at different temperatures. At 260 K, they reach the highest at 0.656 ± 0.12 and 0.822 ± 0.013 Å/ns for the basal and prism1 surfaces, respectively. The existence of a maximum growth rate below the melting point of ice had been previously confirmed in Ref.⁴⁷. They evaluated the effects of the different system sizes (all three bulk systems containing a basal liquid-ice interface in the middle are approximately 110 Å long, with X and Y dimensions of 18×16 , 23×23 , and 27×31 ²) on ice growth rates, finding growth rates from 0.7 to 0.9 to 1.1 Å/ns at 10 K below the melting point for the large, medium and small systems. Our trend is consistent with their results, even if they used the TIP4P-2005 model. Montero de Hijes *et al.*⁵⁷ also studied the ice growth rate for the secondary prismatic plane in the bulk system using the TIP4P/Ice model. They found growth rates of about 1 Å/ns at -14 K and 0.5 Å/ns at -25 K, with values that agree with our simulations focusing on the basal and prism1 surfaces. Their simulation model is, however, the ice-water interface inside the bulk, not the ice-QLL

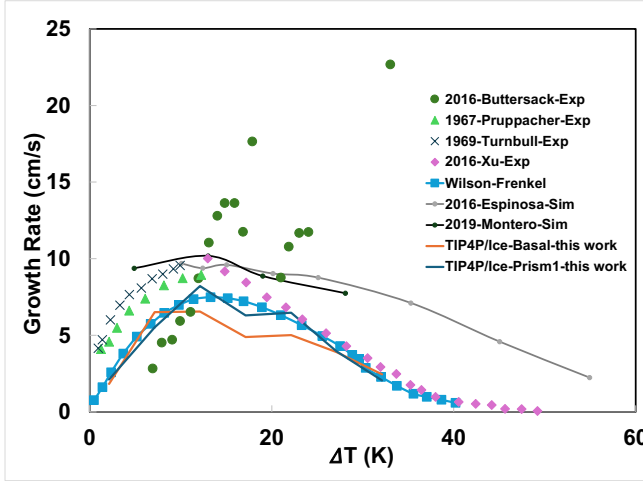


FIG. 4. Comparison of ice Ih growth rates at different surfaces as a function of supercooling, as determined by simulation, theoretical, and experimental results. The experimental results are from Buttersack and Bauerecker⁵⁰ (dark green dots), Pruppacher⁵¹ (green triangles), Turnbull⁵² (grey crosses), and Xu *et al.*⁵³ (pink diamonds). The blue solid line and squares represent the TIP4P/Ice growth rate curve calculated by the WF model^{54,55}. The grey line represents the average growth rate for the three ice Ih surfaces in the bulk system using the TIP4P/Ice model in the NVT ensemble⁵⁶. The black line also represents the average growth rate for the three surfaces of ice Ih in the bulk system using the TIP4P/Ice model in the NVE ensemble⁵⁷. The orange and dark blue lines are the simulation results for the basal and prism1 surfaces in this work using the TIP4P/Ice model.

interface as ours. These previous simulations have claimed to have found a maximum ice growth rate at a certain degree of supercooling. Such a trend also occurs in the mW model, with our simulations showing that the highest mW growth rate occurs at 240 K. A similar behaviour was also found in Espinosa *et al.*'s study for the mW growth rate on the prism2 surface⁵⁶, with the highest value at about 234.6 K⁵⁶; they found that the mW growth rates on the prism2 surface were three orders of magnitude larger than for the TIP4P/Ice model. In our simulations of the basal and prism1 surfaces, we found mW growth rates two orders of magnitude larger than those of TIP4P/Ice.

The Wilson-Frenkel (WF) model^{54,55} includes the effects of the competitive mechanisms leading to the growth rate trend with respect to temperature; it considers diffusive order kinetics as governed by the diffusion coefficient, which is assumed proportional to the addition rate. The predicted growth rate ($R(T)$) is expressed as

$$R(T) = (D(T)/\alpha) [1 - \exp(-\Delta G_{lx}(T)/k_B T)] \quad (1)$$

where $D(T)$ is the diffusion coefficient measured by Price, Ide, and Arata⁵⁸ using NMR spectroscopy, $\Delta G_{lx}(T)$ the chemical potential difference between the solid and the liquid phases, α a molecular dimension (the diameter of a water molecule) and k_B the Boltzmann constant.

We plot in Fig. 4, using a blue solid line with square markers, the results for the WF model with parameters taken from TIP4P/Ice simulations in the bulk system. Specifically, we took the value of $D(T)$ from Ref.^{53,56},

$\Delta G_{lx}(T)_{TIP4P/Ice} = 0.1465 \text{ kcal}\cdot\text{mol}^{-1}$ by averaging the value of $\Delta G_{lx}(T)_{TIP4P/Ice} = 0.147 \text{ kcal}\cdot\text{mol}^{-1}$ in Ref.⁵⁹ and $\Delta G_{lx}(T)_{TIP4P/Ice} = 0.146 \text{ kcal}\cdot\text{mol}^{-1}$ in Ref.⁵⁶ obtained using thermodynamics integration, and $\alpha = 3 \text{ \AA}$ based on the suggestion from Ref.⁵⁷. Our results for the slabs, also shown for comparison in Fig. 4, are qualitatively similar but also capture differences for the different surfaces. Here, the data are shown as a function of the temperature difference from the melting temperature, and rates are in $\text{cm/s} = 10^{-1} \text{\AA/ns}$. Our simulation growth rates for the basal and prism1 surfaces have a similar decreasing trend as other simulations^{56,57} at large supercooling. However, the values differ somewhat because the other two simulations are not for a single basal or prism1 plane; they are averaged to obtain the average growth rate of the three surfaces of ice Ih. That is why the simulation results of the others are slightly larger than our values. Comparison of the TIP4P/Ice model simulations with experimental results shows that the simulated maximum growth rate at -14 K is about 1\AA/ns , which is in good agreement with the experimental observations of Xu *et al.*⁵³, who also suggested a maximum growth rate in their study of nanofilms. Our simulation results are consistent with these experiments at large supercooling, particularly for the growth rate of our prism1 surface. However, the simulated results do not agree with those of Buttersack and Bauerecker⁵⁰, who showed significantly higher growth rates of up to 25 cm/s under similar conditions. However, our simulations showed the same increasing trend at moderate supercooling as Turnbull⁵² and^{51,53} experimental results, except that their experimentally measured growth rate values were slightly larger than ours. Besides, our rates are defined in the approximation where the thermostat makes the system isothermal. In experiments, the latent heat released at the interface as crystallization proceeds must diffuse away from the interface to allow further crystallization, as thermal energy buildup can hinder further crystallization⁶⁰; our simulations do not account for this.

In addition, the TIP4P/Ice growth rate can be qualitatively correlated with the ice crystal morphology change, as illustrated in Fig. S2d. When the ice growth rate on the basal plane is larger than the rate on the prism1, ice crystals will grow with a columnar shape, while when the prism1 rate is larger than the basal one, they will grow like platelets. In the TIP4P/Ice simulations, three crossovers in the rate can be observed. The first crossover occurs close to 240 K, where the rates of basal and prism1 are very similar, with a potential coexistence of plate-like and column-like crystals. Then, with temperature increase, the prism1 rate is larger than the basal one, favouring plate-like shapes. Two switch to column-like and plate-like at a small temperature interval of around 265 K. Although caution has to be considered given the error bars and limitation of the water models, these trends showing an alternation of favourable shapes are qualitatively consistent with the morphology diagram based on experimental evidence^{11,15}. In the case of mW, the prism1 surface always grows faster than the basal one, suggesting the growth of platelet-shaped ice crystals at all temperatures. Our mW simulations also confirmed that the QLL thickness on all three ice Ih surfaces increases

with temperature, with no crossovers between each other.

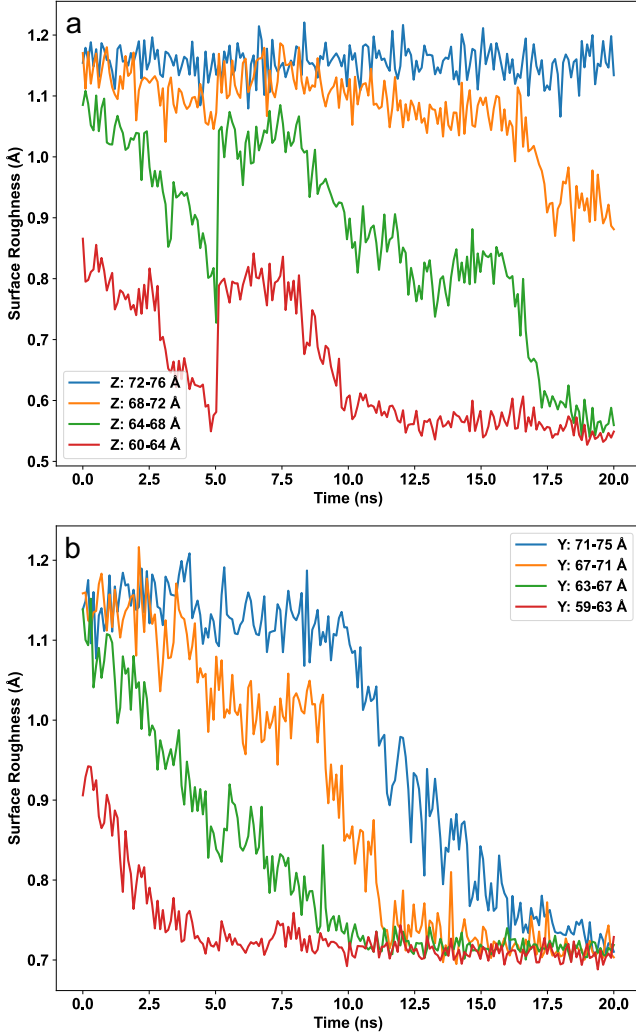


FIG. 5. Time-evolution of the surface roughness of the four ice bilayers above the interface where the melted area meets the ice area on the basal (a) and prism1 (b) surfaces during the TIP4P/Ice crystallization at different times at 260 K.

B. Growth mechanisms of TIP4P/Ice ice Ih at the basal and prism1 QLL/ice interface

The water molecules in the region of the four bilayers melted to enlarge the QLL to study the crystallization process were monitored to study the growth mechanisms of TIP4P/Ice ice Ih at the basal and prism1 QLL/ice interface. The time evolution of the formation of these four ice bilayers at the basal (top panel) and prism1 (bottom panel) surfaces during the TIP4P/Ice crystallization process at 260 K is shown in the SI Fig. S10. We found that the crystallization process on the basal plane follows a 'bilayer-by-bilayer'²⁹ mechanism. The bilayer-by-bilayer pattern for ice crystal growth involves sequentially adding water molecules to the existing ice struc-

ture. This process occurs primarily through a mechanism in which molecules adhere to specific sites at the ice interface, forming a new layer that spreads laterally across the crystal. Growth proceeds uniformly as each layer completes before a new one starts. This can be seen in the first bilayer at 11 ns, the second bilayer at 18.4 ns, and the third bilayer at 23.4 ns. The first bilayer is ordered as the simulation progresses to 11 ns, while most of the second bilayer's molecular state remains disordered. As the simulation continues to 18.4 ns, the second bilayer completes its crystallization and becomes ordered. Although the third bilayer of water molecules is partially ordered with a few ice-like molecules, most of the area remains liquid-like. When the simulation reaches 23.4 ns, the third layer of water molecules completes crystallization and becomes ordered, but the fourth bilayer of water molecules only has a few ice-like molecules. These behaviours reflect the bilayer-by-bilayer growth mechanism on the basal surface.

On the contrary, the prism1 plane follows the mechanism of a 'collected molecule'²⁹ mechanism, which refers to a process in ice crystal growth where molecules adhere to a surface in a stepwise manner, in agreement with the observations by Nada and Furukawa²⁹. The structures at 8.8 ns, 11.9 ns and 15.6 ns for the prism1 plane in the bottom panels in Fig. S10 reflect the 'collected molecule' growth mechanisms. At 8.8 ns, the first bilayer completely crystallizes and becomes ordered. At this point, a large part of the second layer becomes ordered, and small amounts of ice-like molecules appear in the third and fourth bilayers. When the simulation progresses to 11.9 ns, the second bilayer is entirely crystallized, the third bilayer is essentially crystallized, and some ice-like molecules even appear in the fourth bilayer. When the simulation reaches 15.6 ns, the third water molecule bilayer has completed the crystallization process, and the fourth bilayer is also mostly crystallized. Through the above analysis and comparison with the growth mechanism of the basal plane, we can conclude that the 'collected molecule' is a sort of three-dimensional growth mode through the longitudinal space. These molecules are collected at the interface and arranged into a structured layer. This mechanism leads to more localized and less uniform growth. Because of this three-dimensional growth mode, the probability of the appearance of ordered ice-like molecules in the longitudinal space increases, and this mechanism also significantly accelerates the growth rate on the prism1 surface.

Since the last water bilayer to crystallize is at the interface with the equilibrium QLL, focusing on the growth process of this final bilayer, could help explain the growth mechanism of ice surfaces. As seen from the number density profiles in the SI Fig. S12, the penultimate bilayer on the basal surface is fully crystallized. It exhibits a bilayer structure with two peaks before the final bilayer crystallizes. After the final bilayer has completely crystallized, the penultimate bilayer maintains the bilayer structure, and the number density does not fluctuate. In contrast, the number density in the region of the subsequent QLL does not change much. This further confirms the bilayer-by-bilayer growth mechanism on the basal surface. Unlike the basal plane, the prism1 surface shows a noticeable increase in the number density of the penultimate bilayer after the final bilayer is wholly crystallized while showing a more clearly

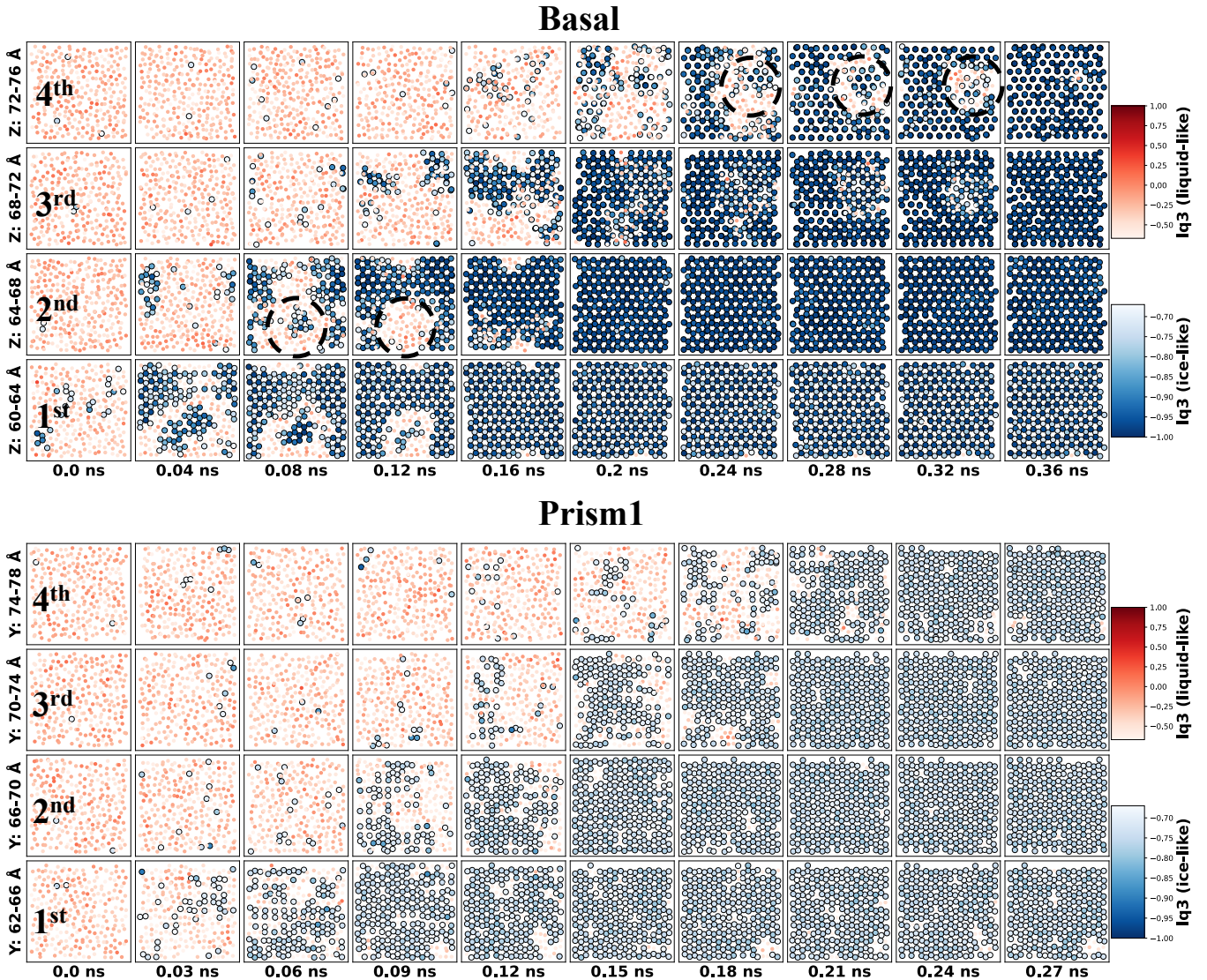


FIG. 6. Time-evolution of the formation of the four ice bilayers above the interface where the melted area meets the area of ice on the basal (top panel) and prism1 (bottom panel) surfaces during the mW crystallization process at 240 K. The darker blue indicates that the molecules are in a more ordered state, i.e., ice-like molecules; the more reddish molecules correspond to a more disordered state, i.e., liquid-like molecules. The oxygen atoms are coloured according to the values of the order parameter l_{q3} with the threshold of -0.67.

defined bilayer structure. At the same time, the molecules in the QLL region have become a bit more ordered, and all these various clues point to a growth mechanism different from the basal surface.

C. Bilayer roughness of TIP4P/Ice ice Ih at the basal and prism1 QLL/ice interface

The degree of order/disorder of the basal and prism1 ice Ih surfaces has been related to the propensity of growing with plate-like or column-like shapes in qualitative agreement with experimental data in molecular dynamics simulations with large surfaces in pure water systems⁶¹ and in the presence

of sodium chloride⁶² through analysis of the roughness. The roughness of the ice surface affects the adsorption of reactive species. It is a factor that influences the growth rate of differently oriented crystal faces, thus controlling the shape of crystals formed by vapour condensation.

Here, we analyzed the time-evolution of the roughness of the four bilayers for the basal and prism1 orientations using the root mean square roughness⁶³,

$$R = \sqrt{\frac{1}{N} \sum_{i=1}^N (z_i - \bar{z})^2} \quad (2)$$

where z_i is the 'height' of a specific oxygen within the bilayer region in the direction orthogonal to the surface, \bar{z} is the average height, and N is the number of points within a given

area.

Fig. 5 shows the time evolution of the roughness of the four bilayers in the basal and prism1 surfaces at specific simulation times. The basal plane initially exhibits a large roughness in the four bilayers because the first bilayer is still in the preparatory stage of crystallization, and the other bilayers are located further away at the upper part of the QLL and also exhibit a large roughness. The first bilayer undergoes crystallization and flattens as the simulation continues, so its roughness decreases. In contrast, the roughness of the second bilayer exhibits a certain degree of decrease, as the water molecules in this layer are required to form this neighbouring ice layer. However, the third and fourth bilayers continue to show greater roughness. When the simulation comes to 18.4 ns, the roughness of the second bilayer decreases considerably to complete the crystallization process. Still, the roughness of the fourth bilayer remains unchanged, except for the third bilayer, which shows a slight decrease in roughness. When the simulation reaches 20 ns, most of the region of the third bilayer has become ordered, i.e., the roughness decreases further, but the roughness of the fourth bilayer remains unchanged. The roughness of the basal plane further confirms that the growth of the basal plane tends to be more of a bilayer-by-bilayer growth pattern and does not perturb the roughness of the other layers significantly. The roughness of the four bilayers on the surface of prism1 in Fig. 5 bottom panel, on the other hand, shows a somehow different trends with time. At the start of the simulation, bilayers show a relatively large roughness because of the disordered local liquid-like environment. As the simulation proceeds, we can see that nearly all the bilayers show a simultaneous decreasing trend in roughness. This reflects that the growth process on the surface of prism1 is that all the molecules in the QLL region are actively involved in the icing of each bilayer process, which is a three-dimensional form of growth mechanism in the presence of large perturbations.

D. Growth mechanisms of mW ice Ih at the basal and prism1 QLL/ice interface

To explain the reason for the fast growth rate of mW, we analyze the MD trajectories at different simulation times for the two surfaces. From Fig. 6, we can conclude that for the mW model, the growth mechanism in both planes is a three-dimensional growth pattern of 'collected molecules,' which explains to some extent why their growth rate is two orders of magnitude of the TIP4P/Ice model. For the basal plane, even though our simulation uses periodic boundary conditions and we cannot define the boundary edges of the plane, we can still conclude that the molecular regularization of the basal surface occurs first at the boundary region of the plane in the top panel of the Fig. 6. The black circle highlighted the center regions. Molecular-ordered and disordered transformations exist in the same black circle at different moments. This reflects the existence of a dislocation correction mechanism⁶⁴ in the growth process of the basal plane. In comparison, the bilayer on the prism1 surface shows homogeneous growth, i.e., the surface

appears flatter. That is to say that during the growth of each layer, defects appear uniformly everywhere in the plane instead of appearing first at the boundaries and then gradually expanding towards the centre to complete the crystallization process, as in the case of the basal plane. Thus, the mW prism1 plane still exhibits a faster growth process because homogeneous growth occurs everywhere in the plane.

IV. CONCLUSIONS

In this work, we systematically investigated crystallization at the ice-QLL interface for the Ih basal and prism1 surfaces with molecular dynamics simulations using the TIP4P/Ice and mW force field in a wide range of temperatures. The crystallization rates obtained with both water models increased with temperature, reaching a maximum and following a downward trend toward the melting temperature. Both the TIP4P/Ice and the mW growth rates peak at 260 K and 240 K, respectively, with mW rates much faster than TIP4P/Ice. The experimental evolution of ice morphologies with temperature at low vapour pressure between column-like and plate-like can be qualitatively correlated with the ice growth rates in the case of TIP4P but not for mW. Order parameters vary with temperature and correlate with the change in ice morphology³⁴. The anisotropic ice growth mechanisms for the two QLL/ice Ih interfaces were discussed, showing that for the TIP4P model, the basal surface follows a bilayer-by-bilayer pattern, while the prism1 obeys a pattern of collected molecule mechanism. For the basal surface, where the roughness of each bilayer decreases gradually, starting with the first bilayer. The roughness of the outer bilayers decreases more slowly, indicating a sequential crystallization process. On the prism1 surface, however, all four bilayers show a simultaneous and consistent decrease in roughness over time. This indicates a three-dimensional growth mechanism where all layers are actively involved in the crystallization process, leading to more significant perturbations in the surface structure.

For the mW model, the growth mechanism for both the basal and prism1 surfaces follows a three-dimensional "collected molecule" pattern, accounting for the significantly faster growth rate than the TIP4P/Ice model. On the basal plane, molecular ordering starts at the boundary region, and a dislocation correction mechanism is at play during the growth process. In contrast, the prism1 surface exhibits homogeneous growth across the entire plane, where defects appear uniformly, resulting in a more efficient crystallization process. Consequently, the prism1 plane shows a faster growth rate due to its uniform defect distribution and simultaneous growth across the surface.

SUPPLEMENTARY MATERIAL

The Supplementary Material includes: the initial and the final structures in a recrystallization simulation at 260 K for the basal and prism1 surfaces (Fig. S1); the time evolution of the excess number of liquid-like molecules Δn_l during the

TIP4P/Ice and mW crystallization simulations for one replica at each simulated temperature and for the basal and prism1 surfaces (Fig. S2); the piecewise linear fitting the time evolution of the Δn_l during the TIP4P/Ice crystallization simulations three replicas of the ice Ih basal and prism1 surfaces from 240 K to 270 K (Fig. S3-S9); the time evolution of the formation of the four ice bilayers above the interface where the melted area meets the area of ice on the basal and prism1 surfaces during the TIP4P/Ice crystallization process at 260 K and 265 K (Fig. S10-S11); the formation of the final layer tightly adhering the QLL on the basal and prism1 surfaces during the TIP4P/Ice crystallization process at 260 K (Fig. S12).

ACKNOWLEDGMENTS

We are grateful for computational support from the UK high-performance computing services ARCHER2, for which access was obtained via the UKCP consortium and funded by EPSRC grants EP/P022472/1 and EP/X035891/1, and the UK Materials and Molecular Modelling Hub for computational resources, which is partially funded by EPSRC (EP/T022213/1). JS was supported by a King's China Scholarship Council PhD studentship.

AUTHOR DECLARATIONS

Conflicts of interest

There are no conflicts of interest to declare.

Author Contributions JS, MF, MS and CM participated in the research design. JS and MF performed the simulations. JS analyzed the data. JS and CM wrote the manuscript. All authors contributed to the discussion of the results and the revision of the manuscript and approved the submitted version.

DATA AVAILABILITY STATEMENT

The data supporting this article is openly available from the King's College London research data repository, KORDS, at <https://doi.org/10.18742/27080410>.

¹T. Sei, T. Gonda, and Y. Arima, "Growth rate and morphology of ice crystals growing in a solution of trehalose and water," *Journal of Crystal Growth* **240**, 218–229 (2002).

²X. Xue, H. Jin, Z. He, and J. Liu, "Quantifying the growth rate and morphology of ice crystals growth in cryoprotectants via high-speed camera and cryomicroscope," *Journal of Heat Transfer* **137** (2015).

³G. C. Sosso, J. Chen, S. J. Cox, M. Fitzner, P. Pedevilla, A. Zen, and A. Michaelides, "Crystal nucleation in liquids: Open questions and future challenges in molecular dynamics simulations," *Chemical Reviews* **116**, 7078–7116 (2016), pMID: 27228560, <https://doi.org/10.1021/acs.chemrev.5b00744>.

⁴K. Padayachee, M. Watt, N. Edwards, and D. Mycock, "Cryopreservation as a tool for the conservation of eucalyptus genetic variability: concepts and challenges," *Southern Forests: a Journal of Forest Science* **71**, 165–170 (2009), <https://doi.org/10.2989/SF.2009.71.2.12.827>.

⁵S. G. Cober, G. A. Isaac, and J. W. Strapp, "Characterizations of aircraft icing environments that include supercooled large drops," *Journal of Applied Meteorology* **40**, 1984 – 2002 (2001).

⁶J. S. Kim and A. Yethiraj, "The effect of salt on the melting of ice: A molecular dynamics simulation study," *The Journal of Chemical Physics* **129**, 124504 (2008), <https://doi.org/10.1063/1.2979247>.

⁷W. Cantrell and A. Heymsfield, "Production of ice in tropospheric clouds: A review," *Bulletin of the American Meteorological Society* **86**, 795 – 808 (2005).

⁸K. S. Carslaw, R. G. Harrison, and J. Kirkby, "Cosmic rays, clouds, and climate," *Science* **298**, 1732–1737 (2002), <https://www.science.org/doi/pdf/10.1126/science.1076964>.

⁹M. S. G. Razul and P. G. K. *, "Computer simulations of heterogeneous crystal growth of atomic systems," *Molecular Physics* **103**, 1929–1943 (2005), <https://doi.org/10.1080/00268970500075396>.

¹⁰D. Rozmanov and P. G. Kusalik, "Temperature dependence of crystal growth of hexagonal ice (ih)," *Phys. Chem. Chem. Phys.* **13**, 15501–15511 (2011).

¹¹K. G. Libbrecht, "Physical dynamics of ice crystal growth," *Annual Review of Materials Research* **47**, 271–295 (2017).

¹²F. F. Abraham, "The phases of two-dimensional matter, their transitions, and solid-state stability: A perspective via computer simulation of simple atomic systems," *Physics Reports* **80**, 340–374 (1981).

¹³K. G. Libbrecht, "An experimental apparatus for observing deterministic structure formation in plate-on-pedestal ice crystal growth," *arXiv preprint arXiv:1503.01019* (2015).

¹⁴M. J. Shultz, "Crystal growth in ice and snow," *Physics Today* **71**, 34–39 (2018).

¹⁵K. G. Libbrecht, "The physics of snow crystals," *Reports on Progress in Physics* **68**, 855 (2005).

¹⁶K. G. Libbrecht, "Physical dynamics of ice crystal growth," *Annual Review of Materials Research* **47**, 271–295 (2017), <https://doi.org/10.1146/annurev-matsci-070616-124135>.

¹⁷Y. Furukawa, M. Yamamoto, and T. Kuroda, "Ellipsometric study of the transition layer on the surface of an ice crystal," *Journal of crystal growth* **82**, 665–677 (1987).

¹⁸J. A. Raymond, P. Wilson, and A. L. DeVries, "Inhibition of growth of nonbasal planes in ice by fish antifreezes," *Proceedings of the National Academy of Sciences* **86**, 881–885 (1989).

¹⁹Y. Furukawa and S. Kohata, "Temperature dependence of the growth form of negative crystal in an ice single crystal and evaporation kinetics for its surfaces," *Journal of crystal growth* **129**, 571–581 (1993).

²⁰D. A. Vorontsov, G. Sazaki, E. K. Titaeva, E. L. Kim, M. Bayer-Giraldi, and Y. Furukawa, "Growth of ice crystals in the presence of type iii antifreeze protein," *Crystal Growth & Design* **18**, 2563–2571 (2018).

²¹M. Bayer-Giraldi, G. Sazaki, K. Nagashima, S. Kipfstuhl, D. A. Vorontsov, and Y. Furukawa, "Growth suppression of ice crystal basal face in the presence of a moderate ice-binding protein does not confer hyperactivity," *Proceedings of the National Academy of Sciences* **115**, 7479–7484 (2018).

²²G. Sazaki, M. Inomata, H. Asakawa, E. Yokoyama, S. Nakatsubo, K.-i. Murata, K. Nagashima, and Y. Furukawa, "In-situ optical microscopy observation of elementary steps on ice crystals grown in vapor and their growth kinetics," *Progress in Crystal Growth and Characterization of Materials* **67**, 100550 (2021).

²³G. Miyamoto, A. Kouchi, K.-i. Murata, K. Nagashima, and G. Sazaki, "Growth kinetics of elementary spiral steps on ice prism faces grown in vapor and their temperature dependence," *Crystal growth & design* **22**, 6639–6646 (2022).

²⁴M. A. Carignano, P. B. Shepson, and I. S. *, "Molecular dynamics simulations of ice growth from supercooled water," *Molecular Physics* **103**, 2957–2967 (2005), <https://doi.org/10.1080/00268970500243796>.

²⁵H. Nada and Y. Furukawa, "Anisotropy in growth kinetics at interfaces between proton-disordered hexagonal ice and water: A molecular dynamics study using the six-site model of h2o," *Journal of Crystal Growth* **283**, 242–256 (2005).

²⁶M. S. G. Razul and P. G. Kusalik, "Crystal growth investigations of ice/water interfaces from molecular dynamics simulations: Profile functions and average properties," *The Journal of Chemical Physics* **134**, 014710 (2011), <https://doi.org/10.1063/1.3518984>.

²⁷M. Seo, E. Jang, K. Kim, S. Choi, and J. S. Kim, "Understanding anisotropic growth behavior of hexagonal ice on a molecular scale: A molecular dynamics simulation study," *The Journal of Chemical Physics* **137**, 154503 (2012), <https://doi.org/10.1063/1.4759113>.

²⁸P. Montero de Hijes, J. R. Espinosa, C. Vega, and E. Sanz, "Ice growth rate: Temperature dependence and effect of heat dissipation," *The Journal of Chemical Physics* **151**, 044509 (2019), <https://doi.org/10.1063/1.5103273>.

²⁹H. Nada and Y. Furukawa, "Anisotropic growth kinetics of ice crystals from water studied by molecular dynamics simulation," *Journal of Crystal Growth* **169**, 587–597 (1996).

³⁰H. Nada and Y. Furukawa, "Anisotropy in molecular-scaled growth kinetics at ice–water interfaces," *The Journal of Physical Chemistry B* **101**, 6163–6166 (1997), <https://doi.org/10.1021/jp963173c>.

³¹M. Matsumoto, S. Saito, and I. Ohmine, "Molecular dynamics simulation of the ice nucleation and growth process leading to water freezing," *Nature* **416**, 409–413 (2002).

³²E. B. Moore and V. Molinero, "Ice crystallization in water's "no-man's land,"" *The Journal of Chemical Physics* **132**, 244504 (2010), <https://doi.org/10.1063/1.3451112>.

³³V. Molinero and E. B. Moore, "Water modeled as an intermediate element between carbon and silicon," *The Journal of Physical Chemistry B* **113**, 4008–4016 (2009).

³⁴J. Shi, M. Fulford, H. Li, M. Marzook, M. Reisjala, M. Salvalaglio, and C. Molteni, "Investigating the quasi-liquid layer on ice surfaces: a comparison of order parameters," *Physical Chemistry Chemical Physics* **24**, 12476–12487 (2022).

³⁵J. Abascal, R. G. Fernandez, L. MacDowell, E. Sanz, and C. Vega, "Ice: A fruitful source of information about liquid water," *Journal of Molecular Liquids* **136**, 214–220 (2007).

³⁶J. L. Abascal and C. Vega, "A general purpose model for the condensed phases of water: Tip4p/2005," *The Journal of Chemical Physics* **123**, 234505 (2005).

³⁷N. Grishina and V. Buch, "Structure and dynamics of orientational defects in ice i," *The Journal of Chemical Physics* **120**, 5217–5225 (2004).

³⁸T. Kling, F. Kling, and D. Donadio, "Structure and dynamics of the quasi-liquid layer at the surface of ice from molecular simulations," *The Journal of Physical Chemistry C* **122**, 24780–24787 (2018).

³⁹S. Plimpton, "Fast parallel algorithms for short-range molecular dynamics," *Journal of Computational Physics* **117**, 1–19 (1995).

⁴⁰G. A. Tribello, M. Bonomi, D. Branduardi, C. Camilloni, and G. Bussi, "Plumed 2: New feathers for an old bird," *Computer Physics Communications* **185**, 604–613 (2014).

⁴¹M. Bonomi, D. Branduardi, G. Bussi, C. Camilloni, D. Provasi, P. Raiteri, D. Donadio, F. Marinelli, F. Pietrucci, R. A. Broglia, *et al.*, "Plumed: A portable plugin for free-energy calculations with molecular dynamics," *Computer Physics Communications* **180**, 1961–1972 (2009).

⁴²Blender Online Community, "Blender," (2024).

⁴³J. A. Bender, "Ukichiro nakaya," *Arctic* **15**, 242–243 (1962).

⁴⁴Y. Furukawa and J. S. Wettlaufer, "Snow and ice crystals," *Physics today* **60**, 70–71 (2007).

⁴⁵A. Savitzky and M. J. Golay, "Smoothing and differentiation of data by simplified least squares procedures," *Analytical chemistry* **36**, 1627–1639 (1964).

⁴⁶R. Killick, P. Fearnhead, and I. A. Eckley, "Optimal detection of changepoints with a linear computational cost," *Journal of the American Statistical Association* **107**, 1590–1598 (2012).

⁴⁷D. Rozmanov and P. G. Kusalik, "Temperature dependence of crystal growth of hexagonal ice (i h)," *Physical Chemistry Chemical Physics* **13**, 15501–15511 (2011).

⁴⁸J. Shi, *Modelling the Mechanisms of Ice Crystal Growth at the Molecular Scale*, Ph.D. thesis, King's College London, London, United Kingdom (2024).

⁴⁹V. Molinero and E. B. Moore, "Water modeled as an intermediate element between carbon and silicon," *The Journal of Physical Chemistry B* **113**, 4008–4016 (2009), pMID: 18956896, <https://doi.org/10.1021/jp805227c>.

⁵⁰T. Buttersack and S. Bauerecker, "Critical radius of supercooled water droplets: On the transition toward dendritic freezing," *The Journal of Physical Chemistry B* **120**, 504–512 (2016).

⁵¹H. Pruppacher, "Interpretation of experimentally determined growth rates of ice crystals in supercooled water," *The Journal of Chemical Physics* **47**, 1807–1813 (1967).

⁵²D. Turnbull, "Under what conditions can a glass be formed?" *Contemporary physics* **10**, 473–488 (1969).

⁵³Y. Xu, N. G. Petrik, R. S. Smith, B. D. Kay, and G. A. Kimmel, "Growth rate of crystalline ice and the diffusivity of supercooled water from 126 to 262 K," *Proceedings of the National Academy of Sciences* **113**, 14921–14925 (2016).

⁵⁴H. W. Wilson, "Xx. on the velocity of solidification and viscosity of supercooled liquids," *The London, Edinburgh, and Dublin Philosophical Magazine and Journal of Science* **50**, 238–250 (1900).

⁵⁵J. Frenkel, *Kinetic theory of liquids* (The Clarendon Press, Oxford, 1946).

⁵⁶J. Espinosa, C. Navarro, E. Sanz, C. Valeriani, and C. Vega, "On the time required to freeze water," *The Journal of Chemical Physics* **145** (2016).

⁵⁷P. Montero de Hijes, J. Espinosa, C. Vega, and E. Sanz, "Ice growth rate: Temperature dependence and effect of heat dissipation," *The Journal of Chemical Physics* **151** (2019).

⁵⁸W. S. Price, H. Ide, and Y. Arata, "Self-diffusion of supercooled water to 238 K using pgse nmr diffusion measurements," *The Journal of Physical Chemistry A* **103**, 448–450 (1999).

⁵⁹A. Haji-Akbari and P. G. Debenedetti, "Direct calculation of ice homogeneous nucleation rate for a molecular model of water," *Proceedings of the National Academy of Sciences* **112**, 10582–10588 (2015), <https://www.pnas.org/doi/pdf/10.1073/pnas.1509267112>.

⁶⁰M. A. Sánchez, T. Kling, T. Ishiyama, M.-J. van Zadel, P. J. Bisson, M. Mezger, M. N. Jochum, J. D. Cyran, W. J. Smit, H. J. Bakker, *et al.*, "Experimental and theoretical evidence for bilayer-by-bilayer surface melting of crystalline ice," *Proceedings of the National Academy of Sciences* **114**, 227–232 (2017).

⁶¹P. Llombart, E. G. Noya, and L. G. MacDowell, "Surface phase transitions and crystal habits of ice in the atmosphere," *Science Advances* **6**, eaay9322 (2020).

⁶²M. L. Berrens, F. C. Bononi, and D. Donadio, "Effect of sodium chloride adsorption on the surface premelting of ice," *Physical Chemistry Chemical Physics* **24**, 20932–20940 (2022).

⁶³M. Khayet, "Characterization of membrane distillation membranes by tapping mode atomic force microscopy," in *Recent Advances in Multidisciplinary Applied Physics* (Elsevier, 2005) pp. 141–148.

⁶⁴H. Men, "A joint diffusion/collision model for crystal growth in pure liquid metals," *Nature Communications* **15**, 5749 (2024).

⁶⁵A. Shibkov, M. Zheltov, A. Korolev, A. Kazakov, and A. Leonov, "Crossover from diffusion-limited to kinetics-limited growth of ice crystals," *Journal of crystal growth* **285**, 215–227 (2005).

⁶⁶R. Caudron, P.-A. Nicq, and E. Valenza, *Blender 3D: Designing Objects* (Packt Publishing Ltd, 2016).

⁶⁷P. M. Piaggi and M. Parrinello, "Entropy based fingerprint for local crystalline order," *The Journal of Chemical Physics* **147**, 114112 (2017).

⁶⁸U. Nakaya, *Snow crystals: natural and artificial* (Harvard University Press, 1954).

⁶⁹J. Frenkel, "Note on a relation between the speed of crystallization and viscosity," *Phisik. Zeit. Sowjetunion* **1**, 498–510 (1932).

⁷⁰B. Slater and A. Michaelides, "Surface premelting of water ice," *Nature Reviews Chemistry* **3**, 172–188 (2019).

⁷¹A. Haji-Akbari and P. G. Debenedetti, "Computational investigation of surface freezing in a molecular model of water," *Proceedings of the National Academy of Sciences* **114**, 3316–3321 (2017), <https://www.pnas.org/doi/pdf/10.1073/pnas.1620999114>.

⁷²H. R. Pruppacher, "Interpretation of experimentally determined growth rates of ice crystals in supercooled water," *The Journal of Chemical Physics* **47**, 1807–1813 (1967), <https://doi.org/10.1063/1.1712169>.

⁷³Y. Furukawa and W. Shimada, "Three-dimensional pattern formation during growth of ice dendrites — its relation to universal law of dendritic growth," *Journal of Crystal Growth* **128**, 234–239 (1993).

⁷⁴J. A. Sellberg, C. Huang, T. A. McQueen, N. Loh, H. Laksmono, D. Schlesinger, R. Sierra, D. Nordlund, C. Hampton, D. Starodub, *et al.*, "Ultrafast x-ray probing of water structure below the homogeneous ice nucleation temperature," *Nature* **510**, 381–384 (2014).

⁷⁵J. Vesenka and Y. Yeh, "Defect site nucleation of microbubbles as a source of dynamic light scattering at the growing ice–water interface," *Journal of Crystal Growth* **108**, 19–24 (1991).

⁷⁶O. A. Karim and A. D. J. Haymet, “The ice/water interface: A molecular dynamics simulation study,” *The Journal of Chemical Physics* **89**, 6889–6896 (1988), <https://doi.org/10.1063/1.455363>.

⁷⁷L. A. Báez and P. Clancy, “Phase equilibria in extended simple point charge ice-water systems,” *The Journal of Chemical Physics* **103**, 9744–9755 (1995), <https://doi.org/10.1063/1.469938>.

⁷⁸M. Carignano, E. Baskaran, P. Shepson, and I. Szleifer, “Molecular dynamics simulation of ice growth from supercooled pure water and from salt solution,” *Annals of Glaciology* **44**, 113–117 (2006).

⁷⁹M. A. Carignano, P. B. Shepson, and I. Szleifer, “Ions at the ice/vapor interface,” *Chemical Physics Letters* **436**, 99–103 (2007).

⁸⁰R. G. Pereyra, I. Szleifer, and M. A. Carignano, “Temperature dependence of ice critical nucleus size,” *The Journal of Chemical Physics* **135**, 034508 (2011), <https://doi.org/10.1063/1.3613672>.

⁸¹L. P. Santos, D. S. da Silva, A. Galembeck, and F. Galembeck, “Electric fields enhance ice formation from water vapor by decreasing the nucleation energy barrier,” *Colloids and Interfaces* **6** (2022), 10.3390/colloids6010013.

⁸²J. D. Honeycutt and H. C. Andersen, “Molecular dynamics study of melting and freezing of small lennard-jones clusters,” *Journal of Physical Chemistry* **91**, 4950–4963 (1987).

⁸³W. Lechner and C. Dellago, “Accurate determination of crystal structures based on averaged local bond order parameters,” *The Journal of Chemical Physics* **129**, 114707 (2008).

⁸⁴A. Stukowski, “Structure identification methods for atomistic simulations of crystalline materials,” *Modelling and Simulation in Materials Science and Engineering* **20**, 045021 (2012).

⁸⁵B. Cheng, G. A. Tribello, and M. Ceriotti, “Solid-liquid interfacial free energy out of equilibrium,” *Physical Review B* **92**, 180102 (2015).

⁸⁶J. R. Espinosa, C. Navarro, E. Sanz, C. Valeriani, and C. Vega, “On the time required to freeze water,” *The Journal of Chemical Physics* **145**, 211922 (2016), <https://doi.org/10.1063/1.4965427>.

Appendix A: SUPPLEMENTARY INFORMATION

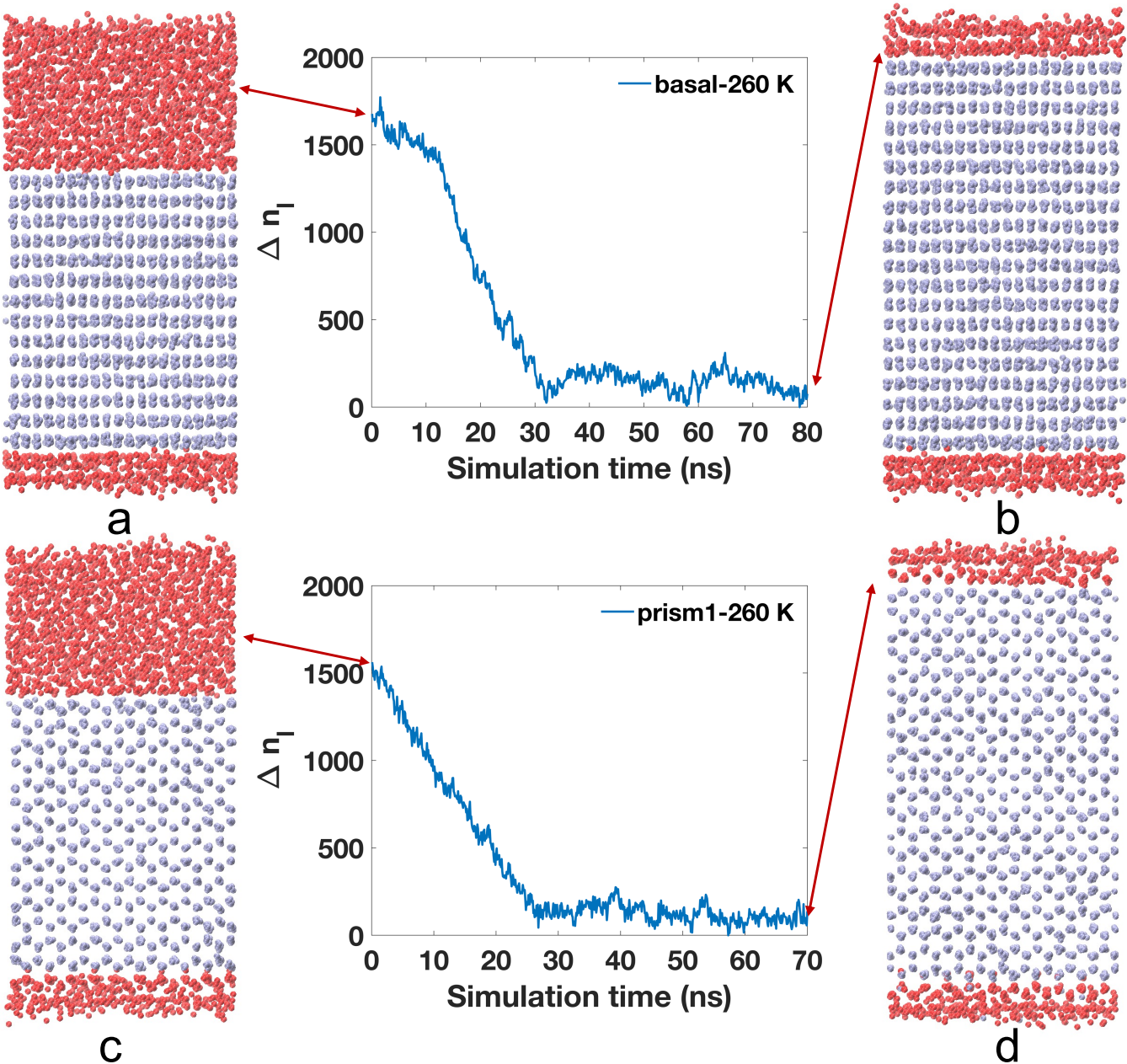


FIG. S1. (a) The initial and (b) the final structures in an 80 ns recrystallization simulation at 260 K for the basal surface. (c) The initial and (d) the final structures in a 70 ns recrystallization simulation at 260 K for the prism1 surface. The liquid-like molecules are coloured in red, and the ice-like molecules are in blue. Only oxygen atoms are shown.

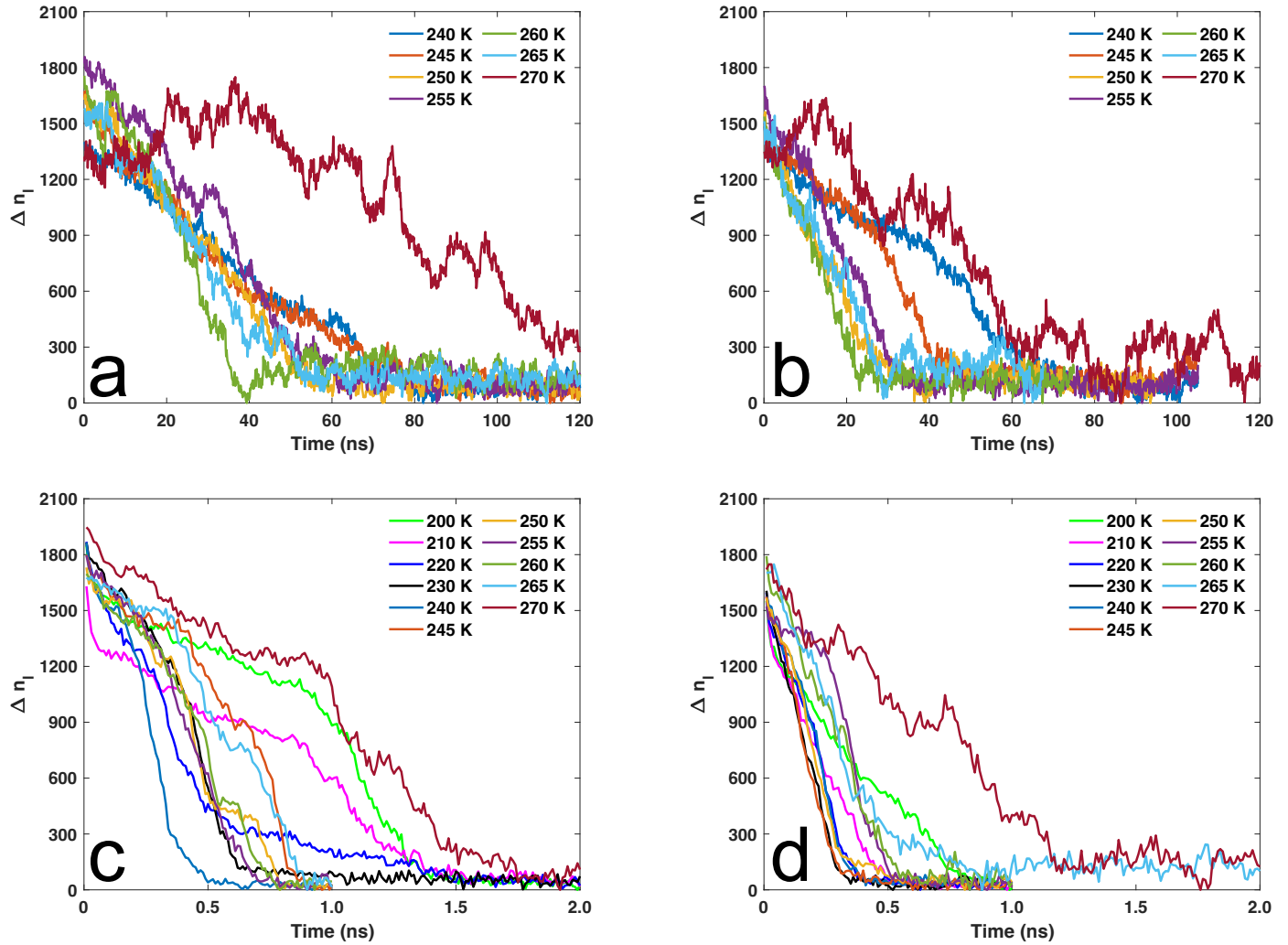


FIG. S2. (a) For the basal surface, the time-evolution of Δn_l during the TIP4P/Ice crystallization simulations for one replica at each simulated temperature and (b) for the prism1 surface. (c) For the basal surface, the time-evolution of Δn_l during the mW crystallization simulations for one replica at each simulated temperature and (d) for the prism1 surface.

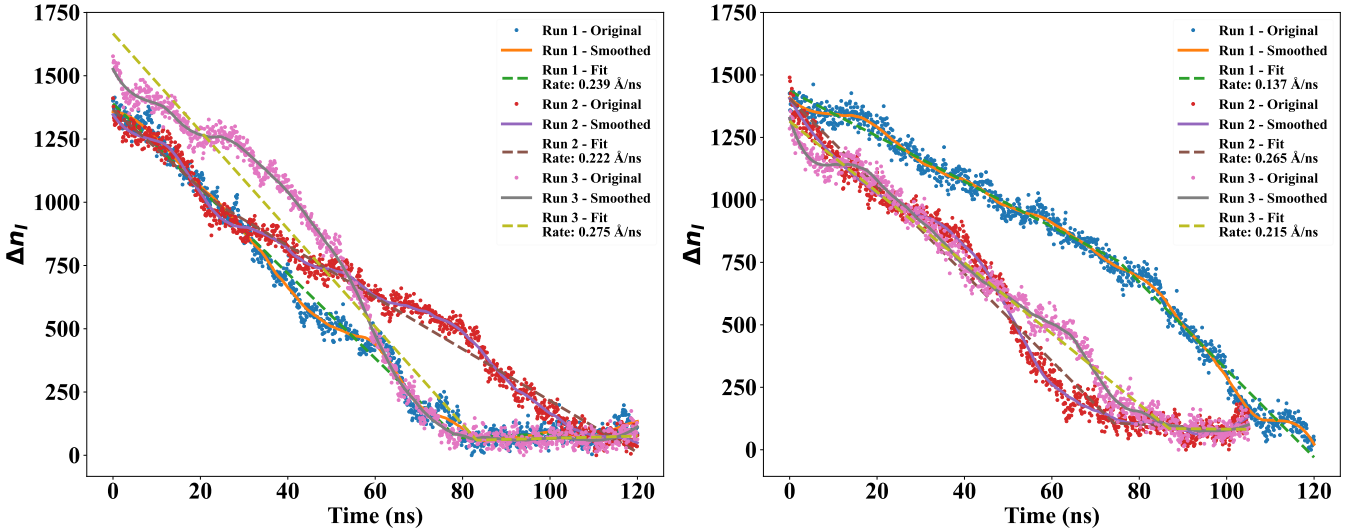


FIG. S3. Time-evolution of the excess number of liquid-like molecules Δn_l during the TIP4P/Ice crystallization simulations three replicas of the ice Ih basal (left panel) and prism1 (right panel) surfaces at 240 K. The piecewise linear fitting technique obtained the ice growth rate. The liquid-like molecules were evaluated using order parameter l_{q3} with a threshold of -0.67.

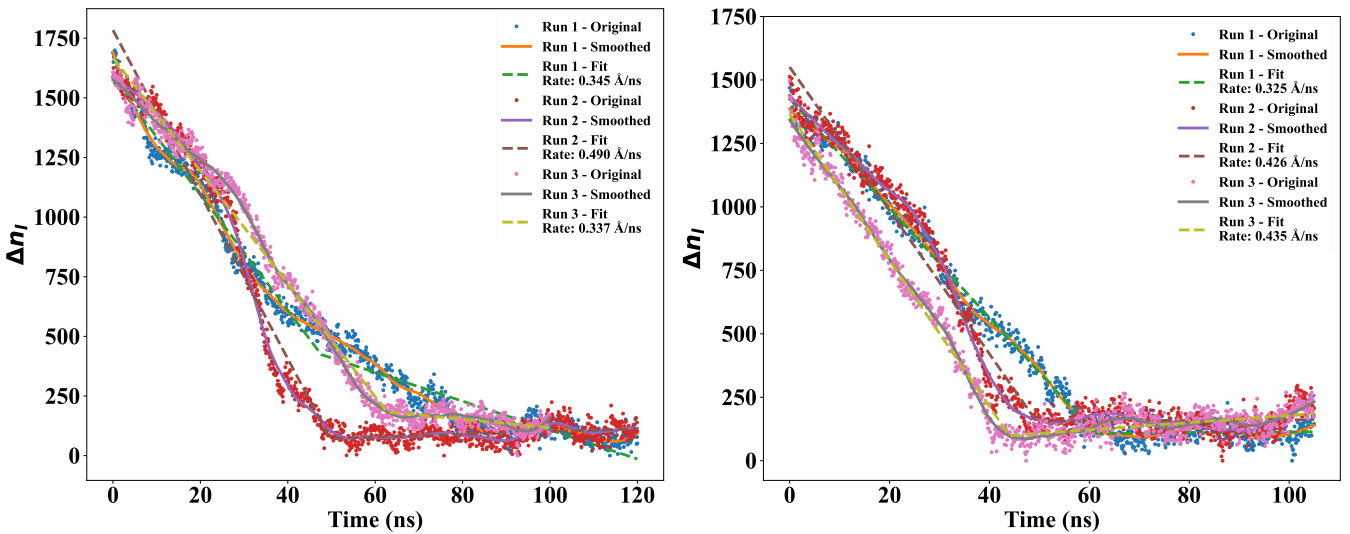


FIG. S4. Time-evolution of the excess number of liquid-like molecules Δn_l during the TIP4P/Ice crystallization simulations three replicas of the ice Ih basal (left panel) and prism1 (right panel) surfaces at 245 K. The piecewise linear fitting technique obtained the ice growth rate. The liquid-like molecules were evaluated using order parameter l_{q3} at a threshold of -0.67.

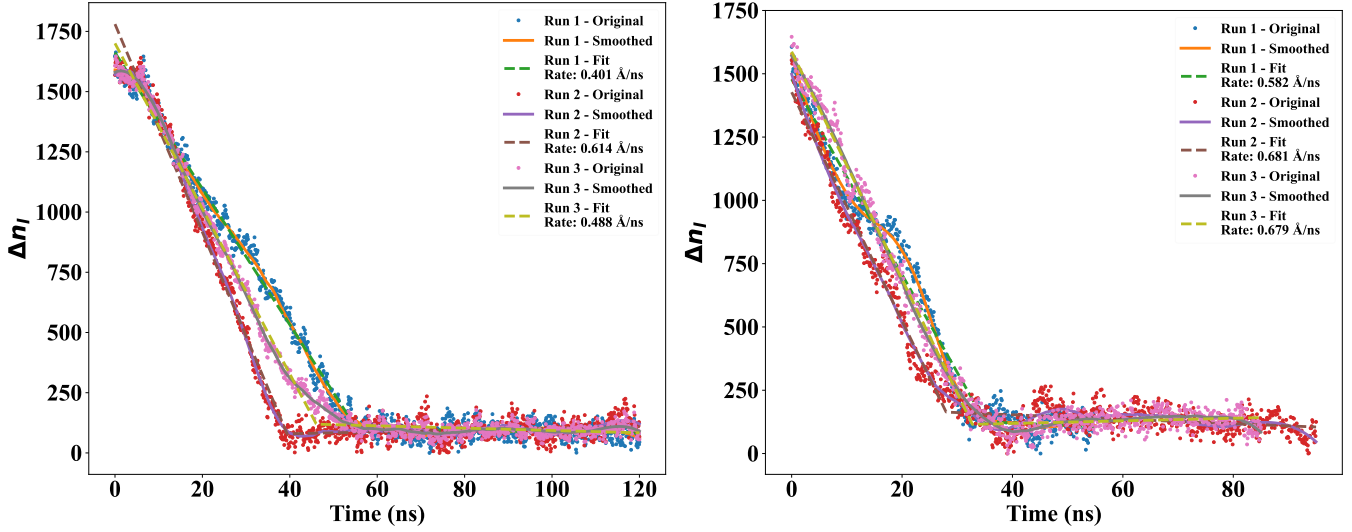


FIG. S5. Time-evolution of the excess number of liquid-like molecules Δn_l during the TIP4P/Ice crystallization simulations three replicas of the ice Ih basal (left panel) and prism1 (right panel) surfaces at 250 K. The piecewise linear fitting technique obtained the ice growth rate. The liquid-like molecules were evaluated using order parameter l_{q3} at a threshold of -0.67.

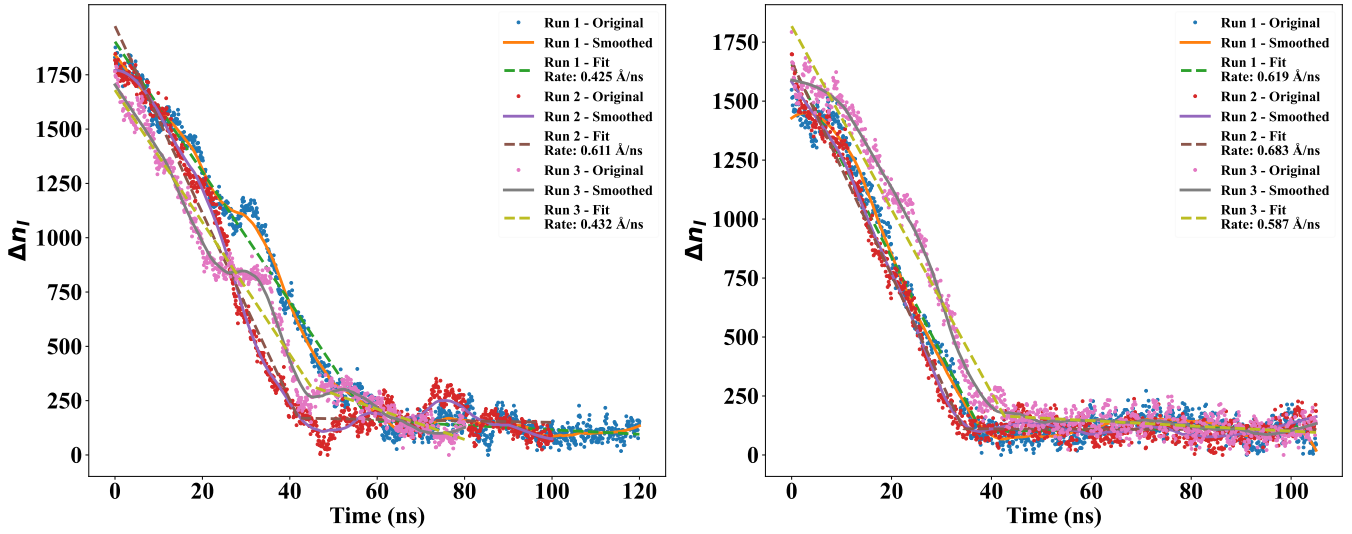


FIG. S6. Time-evolution of the number of excess liquid-like molecules Δn_l during the TIP4P/Ice crystallization simulations three replicas of the ice Ih basal (left panel) and prism1 (right panel) surfaces at 255 K. The piecewise linear fitting technique obtained the ice growth rate. The liquid-like molecules were evaluated using order parameter l_{q3} at a threshold of -0.67.

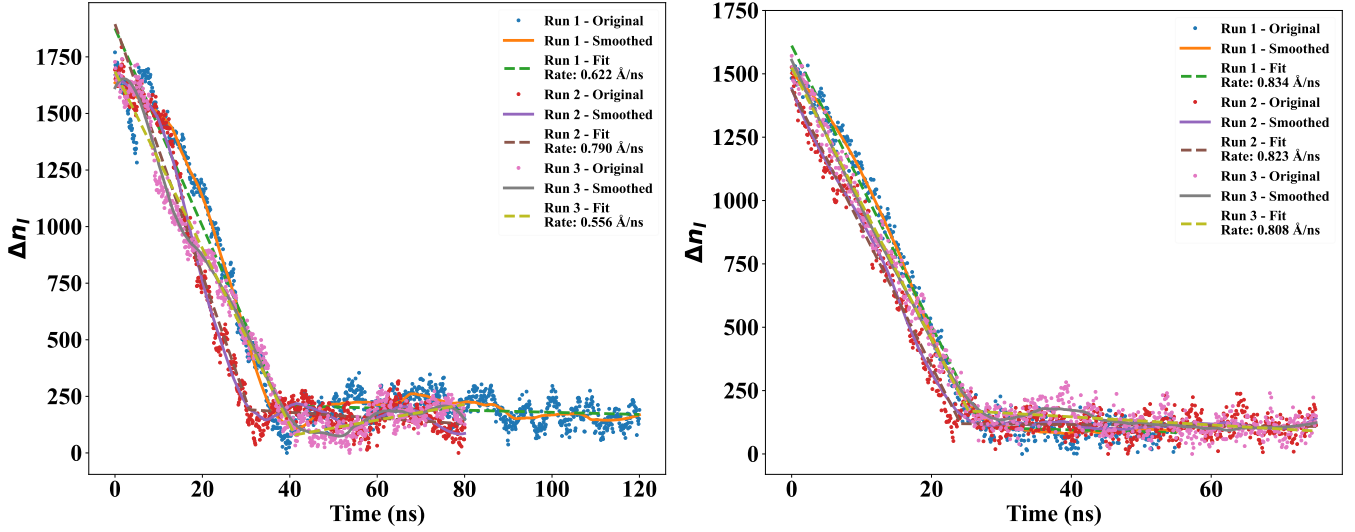


FIG. S7. Time-evolution of the excess number of liquid-like molecules Δn_l during the TIP4P/Ice crystallization simulations three replicas of the ice Ih basal (left panel) and prism1 (right panel) surfaces at 260 K. The piecewise linear fitting technique obtained the ice growth rate. The liquid-like molecules were evaluated using order parameter l_{q3} at a threshold of -0.67.

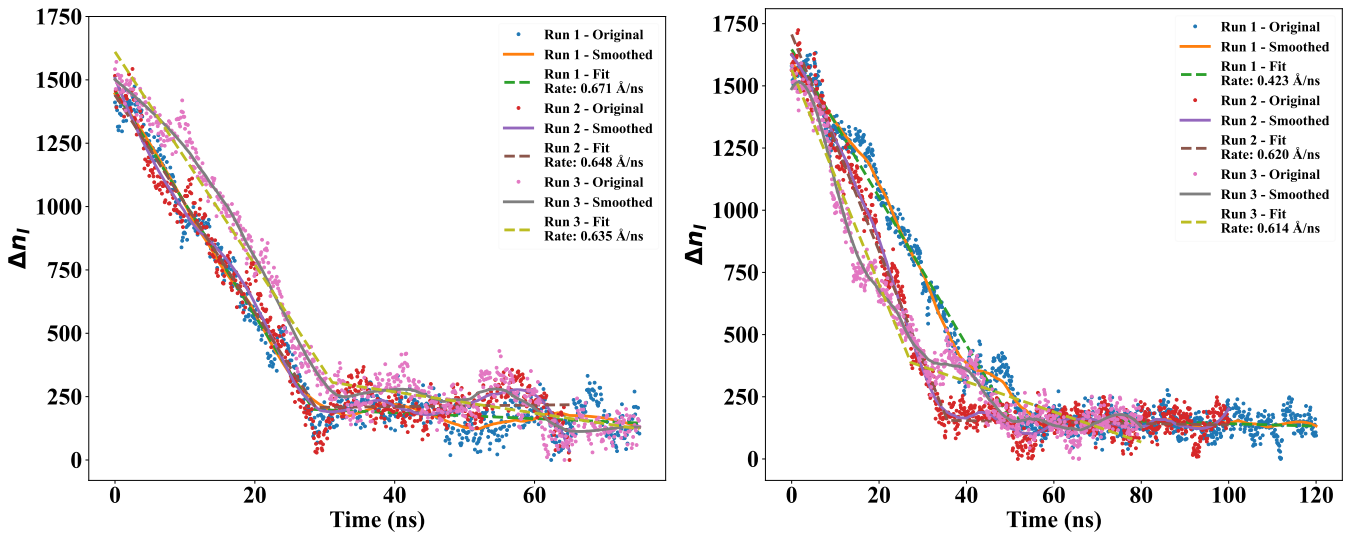


FIG. S8. Time-evolution of the excess number of liquid-like molecules Δn_l during the TIP4P/Ice crystallization simulations three replicas of the ice Ih basal (left panel) and prism1 (right panel) surfaces at 265 K. The piecewise linear fitting technique obtained the ice growth rate. The liquid-like molecules were evaluated using order parameter l_{q3} at a threshold of -0.67.

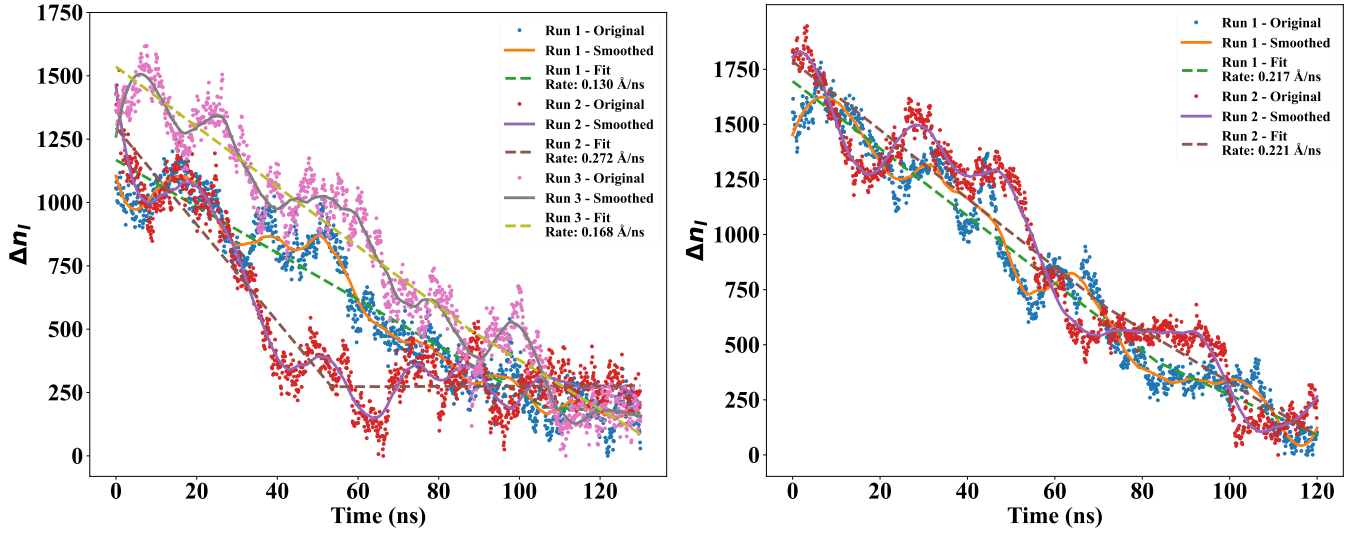


FIG. S9. Time-evolution of the excess number of liquid-like molecules Δn_l during the TIP4P/Ice crystallization simulations three replicas of the ice Ih basal (left panel) and two replicas of the prism1 (right panel) surfaces at 270 K. The piecewise linear fitting technique obtained the ice growth rate. Because there is a long time fluctuation at 270 temperature where there is a large float, some of the initial floating points have been omitted. Because there is a long period of data fluctuation at the beginning, some data points were omitted before fitting relative to other temperatures. The liquid-like molecules were evaluated using order parameter l_{q_3} at a threshold of -0.67.

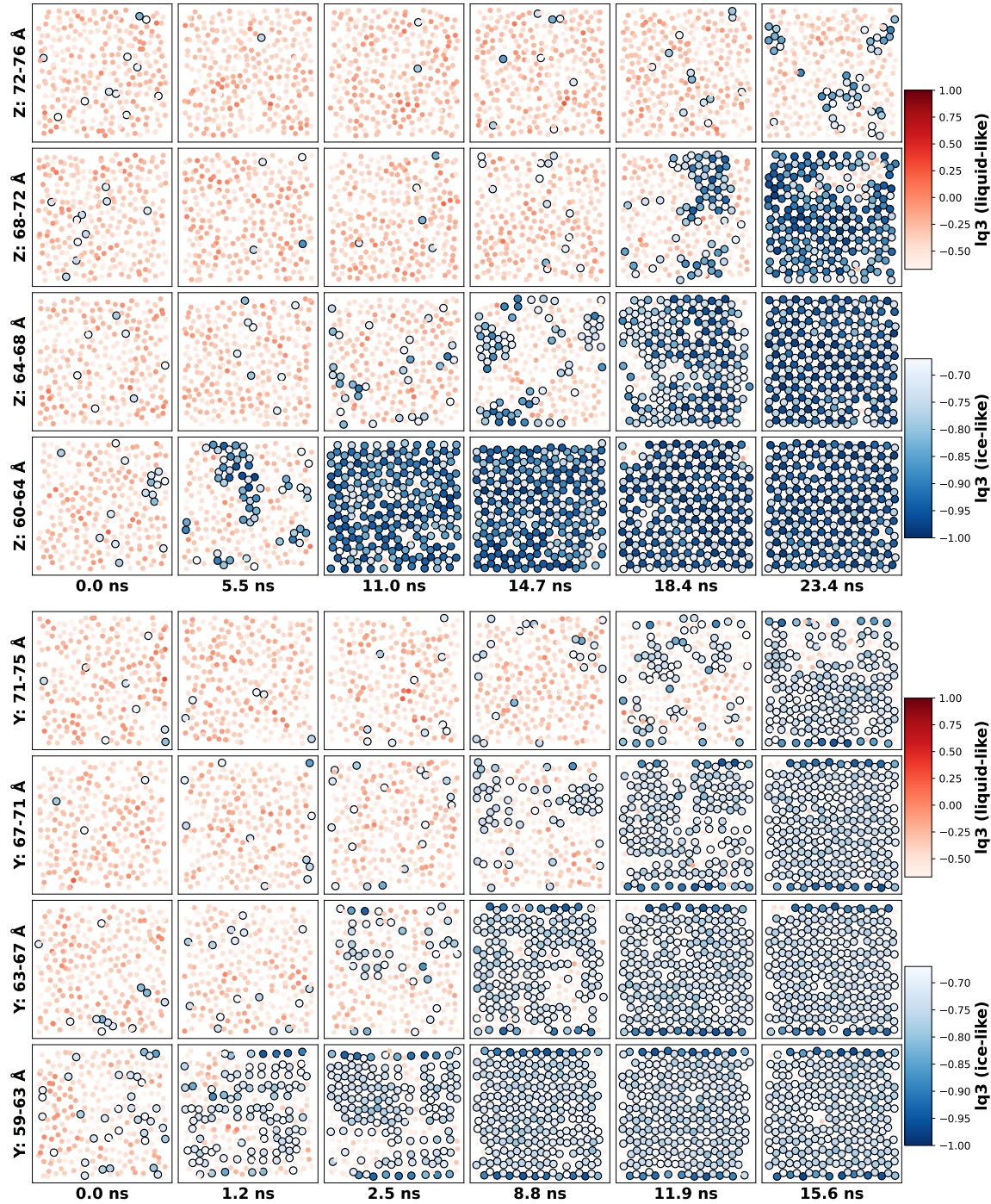


FIG. S10. Time-evolution of the formation of the four ice bilayers ($60-64 \text{ \AA}$, $64-68 \text{ \AA}$, $68-72 \text{ \AA}$, $72-76 \text{ \AA}$, corresponding to the bilayers from 1 to 4 along the model Z direction on the basal plane, respectively; $59-63 \text{ \AA}$, $63-67 \text{ \AA}$, $67-71 \text{ \AA}$, $71-75 \text{ \AA}$, corresponding to the bilayers from 1 to 4 along the model Y direction on the prism1 plane, respectively) above the interface where the melted area meets the area of ice on the basal (top panel) and prism1 (bottom panel) surfaces during the TIP4P/Ice crystallization process at 260 K. The darker blue indicates that the molecules are in a more ordered state, i.e., ice-like molecules; the more reddish molecules correspond to a more disordered state, i.e., liquid-like molecules. The oxygen atoms are coloured according to the values of the order parameter lq_3 with the threshold of -0.67.

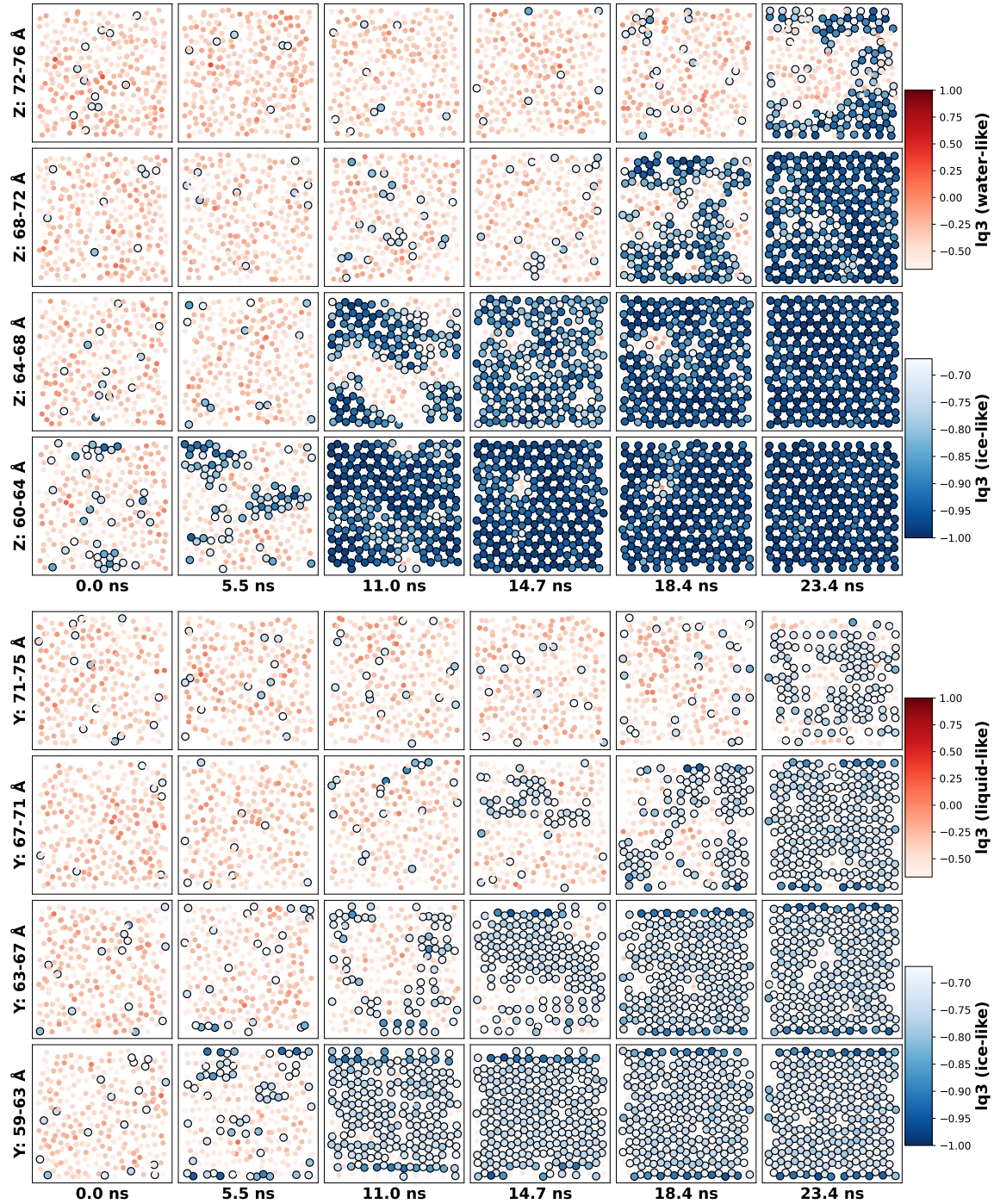


FIG. S11. Time-evolution of the formation of the four ice bilayers above the interface where the melted area meets the ice region for the basal (top panel) and prism1 (bottom panel) surfaces during the TIP4P/Ice crystallization process at 265 K. The darker blue indicates that the molecules are in a more ordered state, i.e., ice-like molecules; the more reddish the dots are, the more disordered the molecules are, i.e., liquid-like molecules. The oxygen atoms are coloured according to the values of the order parameter lq_3 at the threshold of -0.67.

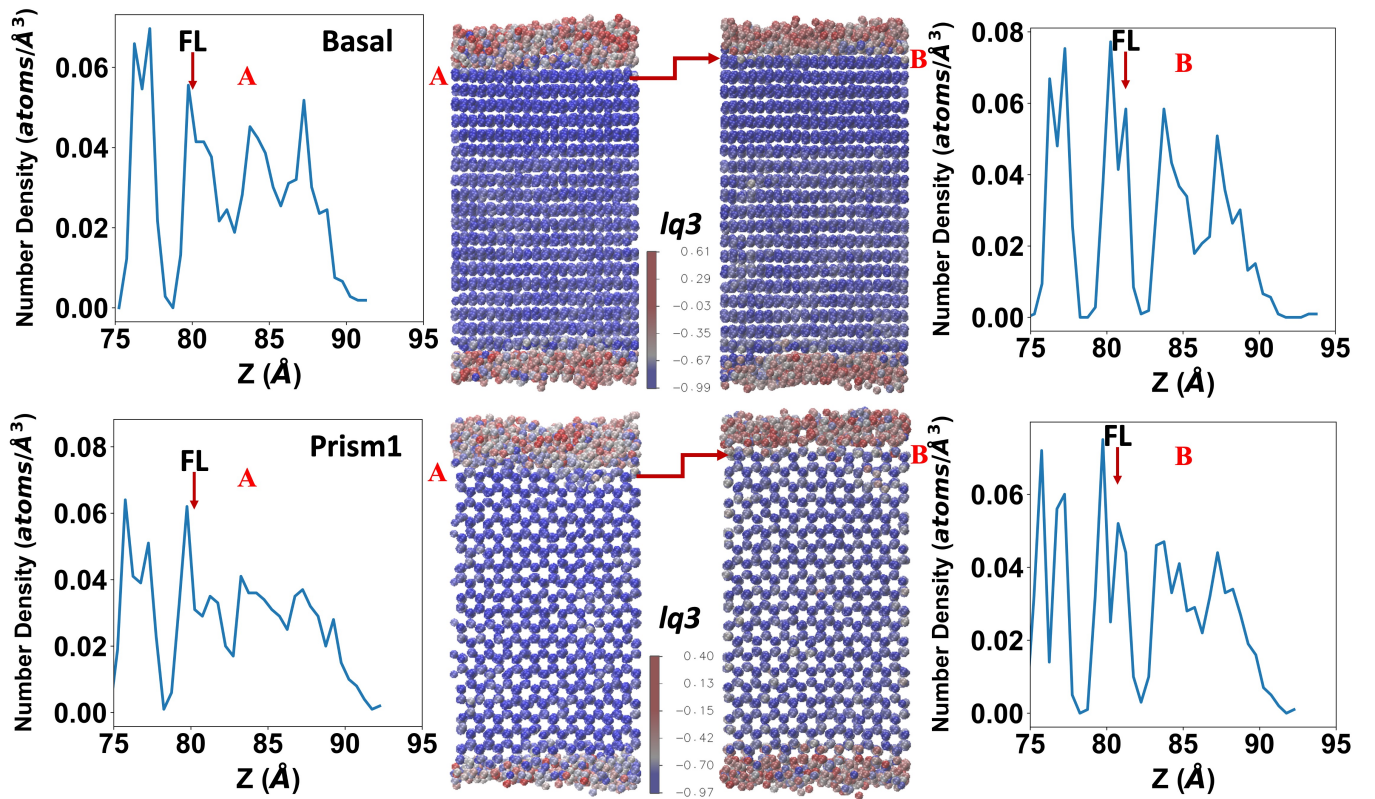


FIG. S12. The formation of the final layer tightly adhering the QLL on the basal (top panel) and prism1 (bottom panel) surfaces during the TIP4P/Ice crystallization process at 260 K. Left panels: the number density profiles of the basal and prism1 surfaces before the final layer freezes and this moment is labelled as state A. Middle panels: The trajectory shows the evolution of the number of liquid-like molecules from the initial state A before the final layer freezes to the state B after complete freezing on the basal and prism1 surfaces. The liquid-like molecules were identified by the order parameter l_{q3} coloured in red. Only oxygen atoms are shown. Right panels: the number density profiles of the basal and prism1 surfaces after the final layer completely freezes, and this moment is labelled as state B. These final layers in the figure for basal and prism1 surfaces at different states are labelled in the figure using the abbreviation FL.